

Constraining dark energy using the cross correlations of weak lensing with post-reionization probes of neutral hydrogen

Chandrachud B. V. Dash,^a Tapomoy Guha Sarkar^{a,1}

^aDepartment of Physics, Birla Institute of Technology and Science, Pilani, 333031, Rajasthan, India.

E-mail: cb.vaswar@gmail.com, tapomoy@pilani.bits-pilani.ac.in

Abstract. We investigate the prospects of detecting the cross correlation of CMBR weak-lensing convergence field with the large scale tracers of the underlying dark matter distribution in the post-reionization epoch. The cross-correlation is then used to make error projections for dark energy equation of state (EoS) for models with a time evolving dark energy. We study the cross-correlation angular power spectrum of the weak-lensing field with the Lyman- α forest and the redshifted HI 21 cm signal from the post reionization epoch. The angular power spectra is expressed as a line of sight average over the tomographic slices. We find that on using multiple 400 hrs observation with an extended uGMRT like instrument or with a BOSS like survey with quasar (QSO) density of 16deg^{-2} the cross-correlation with weak-lensing convergence field covering half the sky can be detected at a very high SNR (> 20). The cross-correlation of weak-lensing with Lyman- α forest allows the $1 - \sigma$ errors on the dark energy EoS parameters for different parametrizations to be constrained at a level of precision comparable to combined Planck+SNIa+BAO+HST projections. The 21-cm weak-lensing cross-correlation is found to provide strong constraints on the present value of the dark energy EoS parameter at 4% for the 7CPL model. The constraints on w_a is comparable ($\sim 12\%$) for models other than the 7CPL model. We also find that the CPL parametrization may not be the best constrained parametrization for dark energy evolution. The cross-correlation of CMBR weak-lensing with the post-reionization probes of neutral hydrogen thus holds the potential to give us valuable understanding about the nature of evolving dark energy.

¹Corresponding author.

Contents

1	Introduction	1
2	Dark energy models	3
3	Weak-lensing convergence power spectrum	4
4	Cross correlation signal	5
4.1	General formulation	7
4.2	Visibility based approach in “flat-sky” approximation	8
5	Cross-correlation of CMBR weak-lensing with Lyman-α forest	10
6	Cross-correlation of CMBR weak-lensing with redshifted 21-cm signal	14
7	Conclusion	18

1 Introduction

A host of independent observations in recent times have indicated that the expansion of the Universe is accelerating [1, 2]. The underlying cause of what is driving this late time acceleration is, however, still an open question. The explanation in the standard paradigm of cosmology assumes a dark energy component with an equation of state (EoS) $p/\rho = w (< -1/3)$. Precision cosmological measurements indicate that the Universe contains approximately $\sim 70\%$ of the energy density in the form of dark energy [3–6] and the remaining $\sim 30\%$ in the form of non-relativistic matter (both baryonic matter and dark matter). A natural candidate for constant dark energy is the cosmological constant Λ . This model with $w = -1$ is well tested by many observations. In this model the cosmological constant Λ is to be interpreted as a non-zero vacuum energy density [7]. While there are theoretical difficulties pertaining to the cosmological constant (like the ‘fine tuning’ problem), recent results from low redshift measurements of H_0 [8] also contradict the Planck-2015 predictions for flat Λ CDM model. Further, there are indications that a varying dark energy model maybe preferable over the concordance Λ CDM model [9] at a high level of statistical significance. Our understanding of the cosmic acceleration thus still remains cloaked in mystery. Dark energy models differing from the standard cosmological constant typically involves a scalar field [10–22] whose dynamics with suitable initial conditions is used to model the cosmic acceleration. It is generally a difficult program to constrain the immense diversity of such scalar field models from observations. It is convenient to use some parametrization of these models which mimic their general behaviour. The dynamic EoS with $p/\rho = w(z)$ is one such commonly used parametrization [17, 23–26]. The most popular and widely used parametrization of the EoS is a two-parameter model by Chavallier-Linder-Polarski (CPL), [26, 27]. In this study we shall also use two important variants of the CPL model called the 7CPL model [25] and Brboza-Alcaniz (BA) model [28].

Weak gravitational lensing by intervening large scale structure [29–31] distorts the images of distant background sources, over large angular scales. This is caused by the deflection

of light by the fluctuating gravitational field created by the intervening overdensity field. Precise quantitative measurement of these distortions opens a window towards our understanding of the large scale matter distribution and geometry of the Universe. Late time cosmic history is governed largely by dark energy, either through a modification of the growing mode of density perturbations or through clustering properties of dark energy or both. Weak-lensing studies can be used to impose constraints on dark energy models [32, 33] since the lensing distortions manifest as a line of sight integral of a ‘kernel’ which is sensitive to background evolution and structure formation. Weak-lensing also distorts the CMBR photon distribution and manifests as secondary anisotropy in the CMBR maps [34]. The CMBR temperature and polarization maps may be used to extract the effect of lensing [35–37]. Delensing of the CMBR is crucial in quantifying the imprint of gravitational waves in the B modes [38].

Neutral hydrogen (HI) in the post-reionization epoch ($z < 6$) [39–43] is housed in two important astrophysical systems of interest. The bulk of the neutral gas is found in the dense self shielded Damped Lyman- α (DLA) systems [44, 45]. These DLA clouds are the source of the redshifted 21-cm signal, to be seen in emission. Intensity mapping of the large scale HI distribution using observations the redshifted 21-cm radiation [46, 47] aims to map out the collective diffuse emission without resolving the individual DLA sources [48]. The statistics of these intensity maps is a potentially rich probe of cosmological background evolution and large scale structure formation [49–52]. Several studies look at the possibility of using 21-cm intensity mapping to constrain dark energy models [53, 54]. It is also a key science goal of many radio telescopes like the GMRT ¹ OWFA ², MEERKAT ³, MWA ⁴, CHIME ⁵, and SKA ⁶ to detect the cosmological 21-cm signal for a tomographic imaging [55] at observing frequencies $\nu \leq 1420\text{MHz}$.

The Lyman- α system comprises of the diffuse HI in the dominantly ionized post-reionization inter galactic medium (IGM), which produces distinct absorption features in the spectra of background QSOs. These absorption features known as the Lyman- α forest, provides one dimensional maps of the underlying HI fluctuation field along QSO sight lines. The Lyman- α forest is known to be a powerful cosmological probe [56–62]. The Baryon Oscillation Spectroscopic Survey (BOSS) [63, 64] has measured the BAO imprint on the Lyman- α forest. The eBOSS ⁷ survey is expected to cover 6000 square degrees and acquire data for 500,000 quasars in the redshift range $0.8 < z < 3.5$. The high number density of QSOs in this survey and the high signal to noise ratio (SNR) measurement of the Lyman- α spectra allows 3D analysis [65, 66] and powerful investigation of the cosmological dark sector [67, 68].

Large scale numerical simulations indicate that on large cosmological scales both the Lyman- α forest and the 21-cm signal are biased tracers of the underlying dark matter (DM) distribution [69–73]. This has allowed the possibility of studying cross-correlations between Lyman- α and post reionization 21-cm signal [66, 72, 74–76]. We consider the cross correlation of these post-reionization tracers with the weak-lensing convergence field to constrain dark energy models. The cross-correlation of 21-cm signal and the Lyman- α forest with weak-lensing has been studied earlier [77, 78]. We perform an improved analysis of the angular cross power spectrum for correlations of the CMBR weak lensing convergence field with the

¹<http://gmrt.ncra.tifr.res.in/>

²<https://arxiv.org/abs/1703.00621>

³<http://www.ska.ac.za/meerkat/>

⁴<https://www.mwatelescope.org/>

⁵<http://chime.phas.ubc.ca/>

⁶<https://www.skatelescope.org/>

⁷<https://www.sdss.org/surveys/eboss/>

Lyman- α forest and 21-cm signal for constraining different dark energy parametrizations. We use a visibility based realistic formalism for this purpose. The entire redshift range probed by the Lyman- α and the 21-cm signal is exploited in the present analysis whereby the signal is averaged over redshift bins. Cross-correlating the integrated Lyman- α absorption with weak-lensing convergence has been studied [78]. We extend this idea to the post-reionization signal whereby we consider the signal stacked up over the redshift slices in the observed bandwidth. This is expected to yield greater SNR in detection and more stringent constraints on the dark energy parameters.

The paper is divided as follows. We first consider the dark energy models. We look at the auto correlation convergence power spectrum for CMBR weaklensing. We finally make signal to noise predictions with a Fisher matrix parameter estimation using a visibility based formulation of the cross-correlation of the Lyman- α forest flux and 21-cm signal with the convergence field.

2 Dark energy models

The evolution of the Hubble parameter $H(a)$ for a spatially flat FRW Universe is given by

$$\frac{H(a)}{H_0} = \sqrt{\Omega_{m_0} a^{-3} + (1 - \Omega_{m_0}) \exp \left[-3 \int_1^a da' \frac{1 + w(a')}{a'} \right]} \quad (2.1)$$

where H_0 and Ω_{m_0} denote the Hubble parameter and the matter density parameter respectively at the present epoch and the Universe is assumed to be comprised of non-relativistic matter and a dark energy component with an evolving EoS $w(a)$. We have used the cosmological parameters Planck18 results

$$(\Omega_{m_0}, \Omega_{b_0}, H_0, n_s, \sigma_8, \Omega_K) = (0.315, 0.0496, 67.4, 0.965, 0.811, 0)$$

from [79] in this paper.

Our ignorance about the dynamics of Dark energy is modeled using the EoS parametrization $w(z)$ with $a = 1/(1+z)$. There are innumerable possible choices for $w(z)$. However it has been shown that at most a two-parameter model can be optimally constrained from observations [80].

The model proposed by Chevallier Polarski [26] and Linder [27] gave a phenomenological model-free parametrization to incorporate several features of dark energy. This model has been extensively used by the Dark Energy Task force [81] as the standard two parameter description of dark energy dynamics. The EoS is given by $w_{CPL}(z) = w_0^{CPL} + w_a^{CPL} \frac{z}{1+z}$. This model gives a smooth variation of $w(z) = w_0 + w_a$ at $z \rightarrow \infty$ to $w(z) = w_0$ at $z = 0$. It has also been shown that a wide class of quintessence scalar field models can be mapped into the CPL parametrization [82]. However a better fit to both tracking and thawing class of models require a generalization of the CPL parametrization [83]. We use the following parametrizations in this work.

$$w_{CPL}(z) = w_0^{CPL} + w_a^{CPL} \left(\frac{z}{1+z} \right) \quad (CPL) \quad (2.2)$$

$$w_{7CPL}(z) = w_0^{7CPL} + w_a^{7CPL} \left(\frac{z}{1+z} \right)^7 \quad (7CPL) \quad (2.3)$$

$$w_{BA}(z) = w_0^{BA} + w_a^{BA} \left(\frac{z(1+z)}{1+z^2} \right) \quad (BA) \quad (2.4)$$

Each model is characterized by two constant parameters (w_0, w_a) with w_a quantifying the evolution of dark energy from its present value set by w_0 . The effect of dark energy EoS on observable quantities pertaining to the background cosmological evolution and structure formation is discussed in the Appendix.

3 Weak-lensing convergence power spectrum

We consider the weak-lensing of the Cosmic microwave background radiation (CMBR). Gravitational lensing deflects the photons which are free streaming from the last scattering surface (epoch of recombination $z \sim 1000$) and manifests as a secondary anisotropy in the CMBR temperature maps. The effect of gravitational lensing can be extracted from these maps by constructing various estimators for the convergence field κ through quadratic combination of the (T, E, B) fields [35, 36]. Defining convergence κ as $\kappa = -\frac{1}{2}\nabla \cdot \alpha$ where, α is the total deflection, the convergence power spectrum for the CMBR weak lensing is given by

$$C_{\kappa_{CMB}}^{\ell} = \frac{9}{4} \left(\frac{H_0}{c} \right)^4 \Omega_{m0}^2 \int_0^{\chi_{rec}} \frac{g(\chi)^2}{a^2(\chi)} P \left(\frac{\ell}{\chi}, \chi \right) d\chi. \quad (3.1)$$

If $\chi_{rec} = \chi(z_{rec})$ is the comoving distance to the last scattering surface then the weaklensing geometric kernel $g(\chi)$ is given by

$$g(\chi) = \left(\frac{\chi_{rec} - \chi}{\chi_{rec}} \right) \quad (3.2)$$

We have incorporated the Limber approximation in the above expression.

The Fisher matrix is diagonal for a full sky survey and the noise for the CMBR convergence power spectrum is given by

$$\Delta C_{\kappa_{CMB}}^{\ell} = \sqrt{\frac{2}{(2\ell + 1)}} \left(C_{\kappa_{CMB}}^{\ell} + w^{-1} e^{\ell^2 \sigma_b^2} \right) \quad (3.3)$$

where the first term comes from cosmic variance and the instrumental noise is encapsulated in the weight w and a smoothing determined by the beam width σ_b . We may write $w = (\sigma_{pix}^2 \Omega_{pix})^{-1}$. Here σ_{pix}^2 is the error in each pixel which depends on the sensitivity s and observation time for each pixel t_{pix} as $\sigma_{pix} = s/\sqrt{t_{pix}}$. If the FWHM (full width at half maximum) is denoted by θ_{fwhm} then $\Omega_{pix} = K\theta_{fwhm} \times \theta_{fwhm}$ and $\sigma_b^2 = \theta_{fwhm}^2/8\ln 2$. The conversion factor $K^{-1} = \frac{1}{(2\pi)^2} \int d^2\vec{\ell} \ell^2 C_{\ell}$, where C_{ℓ} denotes the CMB angular power spectrum converts noise in CMBR temperature angular power spectrum to that of convergence angular power spectrum. The factor $(2\ell + 1)$ in the denominator counts the number of samples of $C_{\kappa_{CMB}}^{\ell}$ for a given ℓ . Figure (1) shows the SNR for the CMBR weak-lensing angular power spectrum. We have assumed a CMBPol like experiment with pixel noise of $\sigma_{pix}^2 \approx 1\mu K$ and $\theta_{fwhm} = 3\text{arcmin}$ and $w^{-1} = 7.5\mu K^{-2} \text{deg}^{-2}$ for our analysis [84].

Figure (1) shows the SNR for CMBR weak-lensing convergence angular power spectrum. The sensitivities for different dark energy EoS parameterizations differ by a few percent from the LCDM predictions. However, the sensitivities SNR ~ 20 is good enough to rule out some of the parametrizations at 3σ . But most EoS models remains degenerate to LCDM at these sensitivity levels since the difference of the angular power spectrum is $\sim 1\%$.

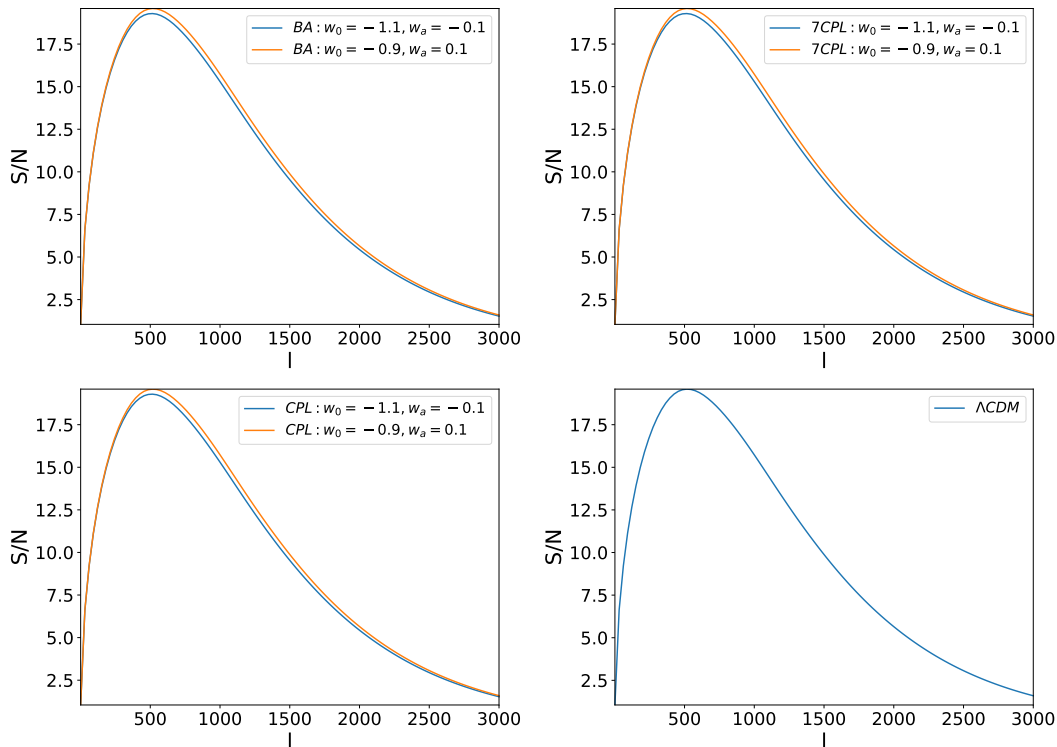


Figure 1: SNR for the CMBR convergence power spectrum for different fiducial dark energy parametrizations.

4 Cross correlation signal

On large scales the Lyman- α forest and the redshifted 21-cm signal from the post reionization epoch are both known to be biased tracers of the underlying dark matter distribution. We denote $\delta\mathcal{F}$ to denote the fluctuations in the Lyman- α transmitted flux $\delta\mathcal{F} = (\mathcal{F} - \bar{\mathcal{F}})/\bar{\mathcal{F}}$. In the post reionization era the neutral fraction remains constant [85–88] and photo-ionization equilibrium leads to a power-law, temperature density relationship [89]. Numerical simulations validate the Fluctuating Gunn-Peterson effect [90–93] whereby it is reasonable to assume that on large scales the smoothed flux fluctuations $\delta\mathcal{F} \propto \delta$, where δ denotes the dark matter overdensity field.

The HI 21-cm emission signal also arises from the same redshift range as the Lyman- α forest. However, they are sourced by the DLAs which are believed to contain most of the HI during the post reionization era. The Lyman- α forest, on the contrary arises from the low density HI in a predominantly ionized IGM. On large scales the HI 21-cm signal also traces the underlying dark matter distribution. We use δ_T to denote the redshifted 21-cm brightness temperature fluctuations.

Including a redshift space distortion we may write both $\delta_{\mathcal{F}}$ and δ_T in Fourier space as

$$\delta_i(\mathbf{r}) = \int \frac{d^3\mathbf{k}}{(2\pi)^3} e^{i\mathbf{k}\cdot\mathbf{r}} \Delta_i(\mathbf{k}). \quad (4.1)$$

where $i = \mathcal{F}$ and T refer to the Ly- α forest transmitted flux and 21-cm brightness temperature

respectively, with

$$\Delta_i(\mathbf{k}) = \mathcal{A}_i[1 + \beta_i\mu^2]\Delta(\mathbf{k}) \quad (4.2)$$

where $\Delta(\mathbf{k})$ is the dark matter density contrast in Fourier space and μ is the cosine of the angle between the line of sight direction $\hat{\mathbf{n}}$ and the wave vector ($\mu = \hat{\mathbf{k}} \cdot \hat{\mathbf{n}}$). β_i is the linear redshift distortion parameter. For the 21-cm signal we have

$$\mathcal{A}_T = 4.0 \text{ mK } b_T \bar{x}_{\text{HI}}(1+z)^2 \left(\frac{\Omega_{b0}h^2}{0.02} \right) \left(\frac{0.7}{h} \right) \left(\frac{H_0}{H(z)} \right) \quad (4.3)$$

where \bar{x}_{HI} is the mean neutral fraction. In the post-reionization epoch $z < 6$, $\Omega_{gas} \sim 10^{-3}$ and the neutral hydrogen fraction remains with a value $\bar{x}_{\text{HI}} = 2.45 \times 10^{-2}$ [85–88]. We may write $\beta_T = f(z)/b_T$ where b_T denotes a bias and $f(z)$ is growth rate of density perturbations. The bias function $b_T(k, z)$ is scale dependent below the Jeans scale. There is also additional scale dependence arising from the fluctuations in the ionizing background [39]. The bias is also a monotonically growing function of redshift [70]. Several studies indicate that on large scales a constant linear bias model is reasonably valid [69–71]. The function $\beta_T(z)$ crucially imprints the dark energy parametrizations through its dependence of $f(z)$ and has a redshift dependence arising from both $f(z)$ and $b_T(z)$.

The interpretation of the linear distortion parameter, $\beta_{\mathcal{F}}$ for the Lyman- α forest, is different owing to the non-linear relation between the Lyman- α transmitted flux and the underlying dark matter density field [93]. Contrary to the parameters for the HI 21-cm signal, the parameters $(\mathcal{A}_{\mathcal{F}}, \beta_{\mathcal{F}})$ are independent of each other and are sensitive to parameters like the IGM temperature-density relationship (γ) and the flux probability distribution function (PDF) of the Lyman- α forest. Analytical work [94] and extensive numerical simulations [72, 95–98] demonstrates that in the absence of primordial non-gaussianity the Lyman- α forest can be described by a linear theory with a scale independent bias on large scales.

We adopt approximate fiducial values $(\mathcal{A}_{\mathcal{F}}, \beta_{\mathcal{F}}) \approx (-0.15, 1.11)$ from the numerical simulations of Lyman- α forest [95]. The bias function b_T is taken from simulation results [70]. These fiducial values of the parameters are used for the Fisher matrix analysis.

We consider the cross-correlation of post-reionization tracers with the weak lensing convergence field. There is a crucial difference between the weak lensing field and the tracer fields. The former measures the integrated effect along the line of sight of a geometric kernel from redshift $z = 0$ to the last scattering surface and, is hence sensitive to the fluctuations of the density field on large scales. The tracers, namely the Lyman- α forest and redshifted 21-cm intensity maps on the contrary are tomographic probes of small scale fluctuations. The cross-correlation thereby quantifies the evolution of small wavelength modes of the fluctuations on top of the long wavelength modes. Further, the noise and systematics which affect the auto-correlation signal appears only in the variance of the cross-correlation and may pose less challenge towards detection of the cross-correlation signal. The 21-cm signal is buried deep under galactic and extra-galactic foregrounds. Even after significant foreground removal, the cosmological origin of the 21 cm signal can only be ascertained only through a cross-correlation.

4.1 General formulation

To formulate the cross-correlation angular power spectrum, we expand the convergence field in terms of spherical harmonics as

$$\kappa(\hat{\mathbf{n}}) = \sum_{\ell, m}^{\infty} a_{\ell m}^{\kappa} Y_{\ell m}(\hat{\mathbf{n}}) \quad (4.4)$$

The expansion coefficients $a_{\ell m}^{\kappa}$ can be obtained by inverting Eq.(4.4) as

$$a_{\ell m}^{\kappa} = \int d\Omega_{\hat{\mathbf{n}}} \kappa(\hat{\mathbf{n}}) Y_{\ell m}^*(\hat{\mathbf{n}}) \quad (4.5)$$

Thus, on using the expression for $\kappa(\hat{\mathbf{n}})$ we have

$$a_{\ell m}^{\kappa} = \int d\Omega_{\hat{\mathbf{n}}} Y_{\ell m}^*(\hat{\mathbf{n}}) \frac{3}{2} \left(\frac{H_0}{c} \right)^2 \Omega_{m_0} \int_0^{\chi_s} g(\chi) \chi \frac{\delta(\chi \hat{\mathbf{n}}, \chi)}{a(\chi)} d\chi \quad (4.6)$$

Writing

$$\delta(\chi \hat{\mathbf{n}}, \chi) = \int \frac{d^3 \mathbf{k}}{(2\pi)^3} e^{i\hat{\mathbf{k}} \cdot \hat{\mathbf{n}} \chi} \Delta(\mathbf{k}) D_+(\chi) \quad (4.7)$$

and using the Raleigh expansion

$$e^{i\hat{\mathbf{k}} \cdot \hat{\mathbf{n}} \chi} = 4\pi \sum_{\ell, m} (-i)^\ell j_\ell(k\chi) Y_{\ell m}^*(\hat{\mathbf{k}}) Y_{\ell m}(\hat{\mathbf{n}}) \quad (4.8)$$

along with the normalization

$$\int d\Omega_{\hat{\mathbf{n}}} Y_{\ell m}^*(\hat{\mathbf{n}}) Y_{\ell m}(\hat{\mathbf{n}}) = 1 \quad (4.9)$$

we have

$$a_{\ell m}^{\kappa} = 4\pi (-i)^\ell \int \frac{d^3 \mathbf{k}}{(2\pi)^3} \int_0^{\chi_s} d\chi \mathcal{A}_\kappa(\chi) D_+(\chi) j_\ell(k\chi) \Delta(\mathbf{k}) Y_{\ell m}^*(\hat{\mathbf{k}}) \quad (4.10)$$

where

$$\mathcal{A}_\kappa(\chi) = \frac{3}{2} \left(\frac{H_0}{c} \right)^2 \Omega_{m_0} \frac{g(\chi) \chi}{a(\chi)} \quad (4.11)$$

For the post reionization tracers Lyman- α and redshifted 21-cm signals we define two fields on the sky by integrating $\delta_i(\chi \hat{\mathbf{n}}, \chi)$ along the radial direction

$$F_i(\hat{\mathbf{n}}) = \frac{1}{\chi_2 - \chi_1} \sum_{\chi_1}^{\chi_2} \Delta\chi \delta_i(\chi \hat{\mathbf{n}}, \chi) \quad (4.12)$$

Previous works [77, 99] consider these fields at a given redshift, where the radial information is retained for tomographic study. The weak-lensing convergence, on the contrary consists of a line of sight integral whereby the redshift information is lost. We consider an average over the signals from redshift slices and thus lose the redshift information but improve the SNR when cross-correlating with the weak-lensing field,

The expansion coefficients for Lyman- α and redshifted 21-cm signals can be generally written as

$$a_{\ell m}^{F_i} = 4\pi(-i)^\ell \int \frac{d^3\mathbf{k}}{(2\pi)^3} \frac{1}{\chi_2 - \chi_1} \sum_{\chi_1}^{\chi_2} \Delta\chi \mathcal{A}_i(\chi) D_+(\chi) \left(j_\ell(k\chi) - \beta_i \frac{d^2 j_\ell(k\chi)}{d(k\chi)^2} \right) \Delta(\mathbf{k}) Y_{\ell m}^*(\hat{\mathbf{k}}) \quad (4.13)$$

Defining the cross-correlation angular power spectrum as

$$\langle a_{\ell m}^\kappa a_{\ell' m'}^{F_i*} \rangle = C_\ell^{\kappa F_i} \delta_{\ell, \ell'} \delta_{m, m'} \quad (4.14)$$

we have

$$C_\ell^{\kappa F_i} = \frac{2}{\pi(\chi_2 - \chi_1)} \int_0^{\chi_s} d\chi \sum_{\chi_1}^{\chi_2} \Delta\chi' \mathcal{A}_\kappa(\chi) D_+(\chi) A_i(\chi') D_+(\chi') \int dk k^2 j_\ell(k\chi) J_\ell(k\chi') P(k) \quad (4.15)$$

where

$$J_\ell(k\chi) = \left(j_\ell(k\chi) - \beta_i \frac{d^2 j_\ell(k\chi)}{d(k\chi)^2} \right) \quad (4.16)$$

Similarly the auto-correlation angular power spectra may be written as

$$C_\ell^{\kappa\kappa} = \frac{2}{\pi} \int_0^{\chi_s} d\chi \int_0^{\chi_s} d\chi' \mathcal{A}_\kappa(\chi) D_+(\chi) A_\kappa(\chi') D_+(\chi') \int dk k^2 j_\ell(k\chi) j_\ell(k\chi') P(k) \quad (4.17)$$

and

$$C_\ell^{F_i F_i} = \frac{2}{\pi(\chi_2 - \chi_1)^2} \sum_{\chi_1}^{\chi_2} \Delta\chi \sum_{\chi_1}^{\chi_2} \Delta\chi' \mathcal{A}_i(\chi) D_+(\chi) A_i(\chi') D_+(\chi') \int dk k^2 J_\ell(k\chi) J_\ell(k\chi') P(k) \quad (4.18)$$

4.2 Visibility based approach in “flat-sky” approximation

Radio interferometric observations of the redshifted 21-cm signal directly measures the complex Visibilities which are the Fourier components of the intensity distribution on the sky. The radio telescope typically has a finite beam which allows us to use the “flat-sky” approximation. Instead of expanding the fields κ and δ_i in the basis of spherical harmonics, we shall now obtain a simplified expression for the angular power spectrum by considering the flat sky approximation whereby we can use the Fourier basis. We define Visibilities as

$$V_{F_i}(\vec{\mathbf{U}}) = \int d^2\vec{\theta} a(\vec{\theta}) F_i(\vec{\theta}) e^{-2\pi i \vec{\mathbf{U}} \cdot \vec{\theta}} \quad (4.19)$$

$$V_\kappa(\vec{\mathbf{U}}) = \int d^2\vec{\theta} \kappa(\vec{\theta}) e^{-2\pi i \vec{\mathbf{U}} \cdot \vec{\theta}} \quad (4.20)$$

where $a(\vec{\theta})$ denotes the beam function of the telescope measuring the angular coverage of the 21-cm or Lyman- α forest survey. Thus

$$V_{F_i}(\vec{\mathbf{U}}) = \frac{1}{\chi_2 - \chi_1} \sum_{\chi_1}^{\chi_2} \Delta\chi \int d^2\vec{\theta} \mathcal{A}_i(\chi) \int \frac{d^2\mathbf{k}_\perp dk_\parallel}{(2\pi)^3} [1 + \beta_i(\chi)\mu^2] \Delta(\mathbf{k}) D_+(\chi) \times e^{ik_\parallel\chi} a(\vec{\theta}) e^{i(\mathbf{k}_\perp\chi - 2\pi\vec{\mathbf{U}}) \cdot \vec{\theta}} \quad (4.21)$$

where $\mu = k_{\parallel}/k$. Performing the $\vec{\theta}$ integral, we have

$$V_{F_i}(\vec{\mathbf{U}}) = \frac{1}{\chi_2 - \chi_1} \sum_{\chi_1}^{\chi_2} \Delta\chi \mathcal{A}_i(\chi) \int \frac{d^2\mathbf{k}_{\perp} dk_{\parallel}}{(2\pi)^3} [1 + \beta_i(\chi)\mu^2] \Delta(\mathbf{k}) D_+(\chi) \times e^{ik_{\parallel}\chi} \tilde{a}_i\left(\frac{\mathbf{k}_{\perp}\chi}{2\pi} - \vec{\mathbf{U}}\right) \quad (4.22)$$

Where the aperture function $\tilde{a}_i(\vec{\mathbf{U}})$ is the Fourier transformation of the telescope beam function $a(\vec{\theta})$. Similarly, for the convergence field we have

$$V_{\kappa}(\vec{\mathbf{U}}) = \int_0^{\chi_s} d\chi \mathcal{A}_{\kappa}(\chi) \int \frac{d^2\mathbf{k}_{\perp} dk_{\parallel}}{(2\pi)^3} \Delta(\mathbf{k}) D_+(\chi) e^{ik_{\parallel}\chi} \delta_D\left(\frac{\mathbf{k}_{\perp}\chi}{2\pi} - \vec{\mathbf{U}}\right) \quad (4.23)$$

where, we have assumed an almost full sky weak-lensing survey. We are interested in the Visibility-Visibility correlation

$$\langle V_{F_i}(\vec{\mathbf{U}}) V_{\kappa}^*(\vec{\mathbf{U}}') \rangle = \frac{1}{\chi_2 - \chi_1} \sum_{\chi_1}^{\chi_2} \Delta\chi \int_0^{\chi_s} d\chi' \mathcal{A}_i(\chi) \mathcal{A}_{\kappa}(\chi') D_+(\chi) D_+(\chi') \int \frac{d^2\mathbf{k}_{\perp} dk_{\parallel}}{(2\pi)^3} e^{ik_{\parallel}(\chi - \chi')} \left[1 + \beta_i(\chi) \frac{k_{\parallel}^2}{k_{\parallel}^2 + \mathbf{k}_{\perp}^2} \right] \tilde{a}_i\left(\frac{\mathbf{k}_{\perp}\chi}{2\pi} - \vec{\mathbf{U}}\right) \delta_D\left(\frac{\mathbf{k}_{\perp}\chi'}{2\pi} - \vec{\mathbf{U}}'\right) P(k) \quad (4.24)$$

Defining $C^{F_i\kappa}(U) = \langle V_{F_i}(\vec{\mathbf{U}}) V_{\kappa}^*(\vec{\mathbf{U}}') \rangle$

$$C^{F_i\kappa}(U) = \frac{1}{\pi(\chi_2 - \chi_1)} \sum_{\chi_1}^{\chi_2} \Delta\chi \int_0^{\chi_s} \frac{d\chi'}{\chi'^2} \mathcal{A}_i(\chi) \mathcal{A}_{\kappa}(\chi') D_+(\chi) D_+(\chi') \int_0^{\infty} dk_{\parallel} \cos k_{\parallel}(\chi - \chi') \left[1 + \beta_i(\chi) \frac{k_{\parallel}^2}{k_{\parallel}^2 + \left(\frac{2\pi\vec{\mathbf{U}}}{\chi'}\right)^2} \right] \tilde{a}_i\left(\frac{\chi - \chi'}{\chi'} \vec{\mathbf{U}}\right) P\left(\sqrt{k_{\parallel}^2 + \left(\frac{2\pi\vec{\mathbf{U}}}{\chi'}\right)^2}\right) \quad (4.25)$$

If the aperture function \tilde{a}_i is peaked, we may approximately write this as

$$C^{F_i\kappa}(U) = \frac{1}{\pi(\chi_2 - \chi_1)} \sum_{\chi_1}^{\chi_2} \frac{\Delta\chi}{\chi^2} \mathcal{A}_i(\chi) \mathcal{A}_{\kappa}(\chi) D_+(\chi)^2 \int_0^{\infty} dk_{\parallel} \left[1 + \beta_i(\chi) \frac{k_{\parallel}^2}{k^2} \right] P(k) \quad (4.26)$$

with $k = \sqrt{k_{\parallel}^2 + \left(\frac{2\pi\vec{\mathbf{U}}}{\chi'}\right)^2}$.

The auto-correlation angular power spectrum may be similarly written as

$$C^{F_i F_i}(U) = \frac{1}{\pi(\chi_2 - \chi_1)^2} \sum_{\chi_1}^{\chi_2} \frac{\Delta\chi}{\chi^2} \mathcal{A}_i(\chi)^2 D_+(\chi)^2 \int_0^{\infty} dk_{\parallel} \left[1 + \beta_i(\chi) \frac{k_{\parallel}^2}{k^2} \right]^2 P(k) \quad (4.27)$$

and

$$C^{\kappa\kappa}(U) = \frac{1}{\pi} \int_0^{\chi_s} \frac{d\chi}{\chi^2} \mathcal{A}_{\kappa}(\chi)^2 D_+(\chi)^2 \int_0^{\infty} dk_{\parallel} P(k) \quad (4.28)$$

We note here that working in the Fourier basis necessarily makes the signal nonergodic when one looks at correlation between two time slices (due to time evolution of all the relevant quantities). Further, one also notes the inseparability of the baseline \mathbf{U} (transverse) from the frequency (radial) in this formalism [100].

The angular power spectrum for two redshifts separated by Δ is known to decorrelate very fast in the radial direction [101]. In this work we consider the summation in Eq (4.12) to extend over redshift slices whose separation is more than the typical decorrelation length. This ensures that in the computation of noise each term in the summation may be thought of as an independent random variable and the mutual covariances between the slices may be ignored. This gives us the SNR in the measurement of $C^{F_i\kappa}(U)$ as

$$\frac{C^{\mathcal{F}_i\kappa}}{\sigma_{\mathcal{F}_i\kappa}} = \frac{C^{\mathcal{F}_i\kappa}\sqrt{2\ell+1}\sqrt{N_c}}{\sqrt{(C^{\kappa\kappa} + \langle N^\kappa \rangle)(C^{F_i F_i} + \langle N^{F_i} \rangle)}} \quad (4.29)$$

where N_c is the number of redshift slices over which the average in Eq (4.12) is taken and $\langle N^{F_i} \rangle$ and $\langle N^\kappa \rangle$ denotes the average of the noise power spectrum for F_i and κ respectively. This variance is used in the Fisher matrix analysis for constraining various dark energy EoS parameters.

The parameters $\mathcal{A}_{\mathcal{F}}$, $\beta_{\mathcal{F}}$, b_T and \bar{x}_{HI} along with the cosmological parameters model the cross-correlation signal. However the parameters $\mathcal{A}_{\mathcal{F}}$, $\beta_{\mathcal{F}}$, b_T and \bar{x}_{HI} are largely uncertain. We perform the Fisher matrix analysis assuming $\mathcal{A}_{\mathcal{F}}$, $\beta_{\mathcal{F}}$, \mathcal{A}_T (related to \bar{x}_{HI}) and β_T (related to b_T) along with the DE EoS parameters w_0 and w_a to be the free parameters. The Fisher matrix is given by

$$\mathbf{F}_{ab} = \sum_{\ell} \frac{1}{\sigma_{\mathcal{F}_i\kappa}^2} \frac{\partial C_{\ell}^{F_i\kappa}}{\partial q_a} \frac{\partial C_{\ell}^{F_i\kappa}}{\partial q_b} \quad (4.30)$$

where we have $q_a = (w_0, w_a, \mathcal{A}_{\mathcal{F}}, \beta_{\mathcal{F}}, \mathcal{A}_T, \beta_T)$. The parameters (w_0, w_a) are different for different models. The Cramer Rao bound gives the errors on the a^{th} parameter $\delta q_a = \sqrt{\mathbf{F}_{aa}^{-1}}$. The error projections on (w_0, w_a) are obtained for different dark energy models by marginalizing over the other parameters.

5 Cross-correlation of CMBR weak-lensing with Lyman- α forest

The redshift distribution of quasars is known to peak in the redshift range $1.5 \leq z \leq 3$ [102]. In our work we consider quasars in these redshifts only and also consider that the Lyman- α forest spectrum for these quasars are measured at a high SNR. We note that for any quasar the region $10,000 \text{ km sec}^{-1}$ blue-wards of the quasar's emission line is contaminated by the quasar's proximity effect and the Stromgen sphere. We exclude this from the Lyman- α forest spectra. We also note that pixels at least $1,000 \text{ km sec}^{-1}$ red-ward of the quasar's needs to be excluded from the spectra to avoid contamination from Lyman- β forest and O-VI lines. Thus, for a quasar at the fiducial redshift $z_Q = 2.5$, the Lyman- α forest can be measured in the redshift range $1.96 \leq z \leq 2.39$ covering a band $z_2 - z_1 = 0.43$. The BOSS survey of $100,000$ square degrees, measures quasar spectra of at least $150,000$ quasars in the redshift range $2.15 < z < 3.5$ which can be used for cross-correlation [103]. We note that for the Lyman- α forest at a redshift z the noise is given by

$$N^{\mathcal{F}} = \frac{1}{\bar{n}_Q} (\sigma_{\mathcal{F}L}^2 + \sigma_{\mathcal{F}N}^2) \quad (5.1)$$

Table 1: The 68% ($1 - \sigma$) Constraints of DE parameters (w_0, w_a) from Lyman- α and convergence cross power spectrum

	$\bar{n}_Q = 8\text{deg}^{-2}$	$\bar{n}_Q = 16\text{deg}^{-2}$	$\bar{n}_Q = 100\text{deg}^{-2}$
BA	$\Delta w_0 = 0.17, \Delta w_a = 0.27$	$\Delta w_0 = 0.15, \Delta w_a = 0.243$	$\Delta w_0 = 0.141, \Delta w_a = 0.192$
CPL	$\Delta w_0 = 0.191, \Delta w_a = 0.57$	$\Delta w_0 = 0.168, \Delta w_a = 0.51$	$\Delta w_0 = 0.121, \Delta w_a = 0.42$
7CPL	$\Delta w_0 = 0.081, \Delta w_a = --$	$\Delta w_0 = 0.079, \Delta w_a = --$	$\Delta w_0 = 0.068, \Delta w_a = --$

where

$$\sigma_{\mathcal{F}L}^2 = \int d^2\mathbf{U} C^{\mathcal{F}\mathcal{F}}(U)$$

and \bar{n}_Q is the angular number density of quasars. The quantity $\sigma_{\mathcal{F}\mathcal{N}}^2$ is a pixel noise contribution. The observations of Lyman- α forest [104, 105] shows that for the Lyman- α forest smoothed over $\sim 50\text{Kms}^{-1}$, the variance of the flux fluctuations has a value $\sigma_{\mathcal{F}L}^2 \approx 0.02$. We adopt this value by choosing the corresponding smoothing scale. We also assume an average $S/N = 5$ for every pixel in the spectra used for cross-correlation. This gives us $\sigma_{\mathcal{F}\mathcal{N}}^2 = 0.04\bar{\mathcal{F}}(z)^{-2} \left(\frac{4.6 \times 10^{-4}}{\Delta z}\right)$. The mean flux $\bar{\mathcal{F}}(z) \sim 1$. The variation of $\bar{\mathcal{F}}(z)$ is however noted [106] The averaging over $N_c = \frac{z_2 - z_1}{\Delta z}$ different slices of redshift gives $\langle N^{\mathcal{F}} \rangle$. The smoothing scale Δz is chosen by noting that at a given redshift z the signal decorrelates over $\Delta z \sim 10^{-3}(1+z)^2 \left(\frac{\ell}{100}\right)^{-0.7}$ [101]. Figure (2) shows the difference of the Lyman- α CMBR convergence cross angular power spectrum for different dark energy EoS parametrizations from the cross angular power spectrum for the LCDM model. We consider Planck sensitivities for the cross-correlation with $\sigma_{pix}\Omega_{pix}^{1/2} = 0.7\mu\text{K.deg}$. For Lyman- α forest we have considered a BOSS like experiment with $\bar{n}_Q = 8, 16$, and 64deg^{-2} for our analysis.

We find that for $\bar{n}_Q = 16\text{deg}^{-2}$ with LCDM fiducial model a peak SNR of ~ 50 (see Fig (3)) is obtained at $\ell \sim 300$. This allows CPL and 7CPL models to be differentiable from the LCDM model at $> 3\sigma$ sensitivity for $\ell > 1000$. The BA model however remains at 1σ from the LCDM and can not be differentiated at these sensitivities. However its variance of the cross-correlation signal is very sensitive to the quasar sampling and dense sampling is expected to improve the sensitivity level for the cross-correlation. A Lyman- α survey with $\bar{n}_Q = 64\text{deg}^{-2}$ the cross correlation has a peak SNR of ~ 80 at $\ell \sim 1200$ [see Fig (3)]. For such sensitivities CPL and 7CPL models can be differentiated at $> 5\sigma$ for $\ell > 1500$. The best case scenario is shown in the last in figure which at $\bar{n}_Q \sim 100\text{deg}^{-2}$. The Fisher matrix in Eq (4.30) is used to put constraints on the dark energy parameters. We have assumed that other cosmological parameters are well constrained from CMBR observations and focus only on the dark energy EoS parameters. Fig (4) shows the constraints on the parameters in the $w_0 - w_a$ plane. The contours correspond to also show the 68% and 95% marginalized confidence intervals for the parameters w_0 and w_a .

The table (1) shows the $1 - \sigma$ errors on EoS parameters. We find that if dark energy is described by CPL parametrization, the constraint in $w_0 - w_a$ space is competitive with the Planck+Bao+Supernova+HST for CPL parametrization [107].

We also find that for the 7CPL parametrization, the parameter w_a can not be constrained. However, for 7CPL parametrization we can constrain w_0 much better than CPL or BA. Thus we note that for the measurement of the present day value of the dark energy equa-

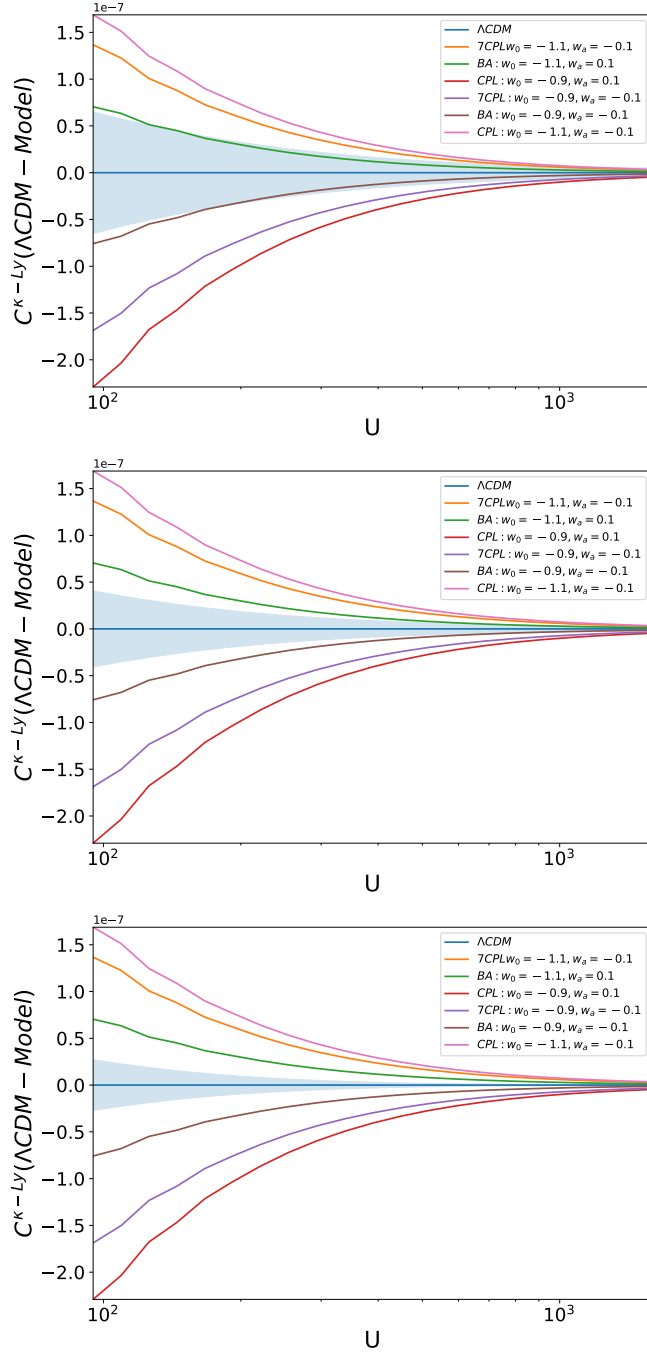


Figure 2: The difference of the Lyman- α forest - CMBR convergence cross power spectrum for different fiducial dark energy parametrizations from the the Λ CDM model. The $1 - \sigma$ error is shown by the shaded region. The first and the second figure corresponds to a quasar number density of $\bar{n}_Q = 16\text{deg}^{-2}$ and $\bar{n}_Q = 64\text{deg}^{-2}$ respectively. The last figure shows the best case scenario in the cosmic variance limit of no observational noise.

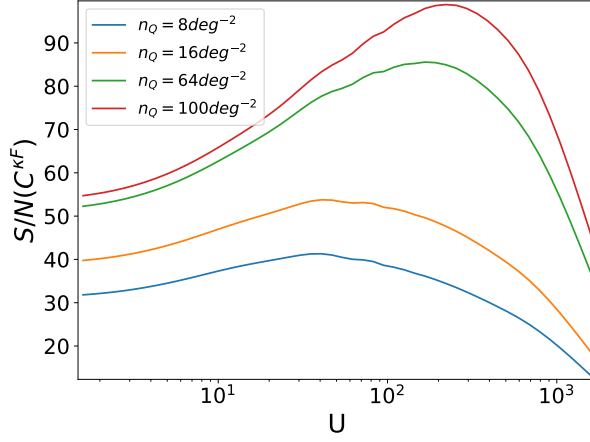


Figure 3: Signal to Noise ratio for the Convergence-Lyman- α angular power spectrum for the fiducial LCDM model for $\bar{n}_Q = 8, 16, 64, 100 \text{ deg}^{-2}$ respectively.

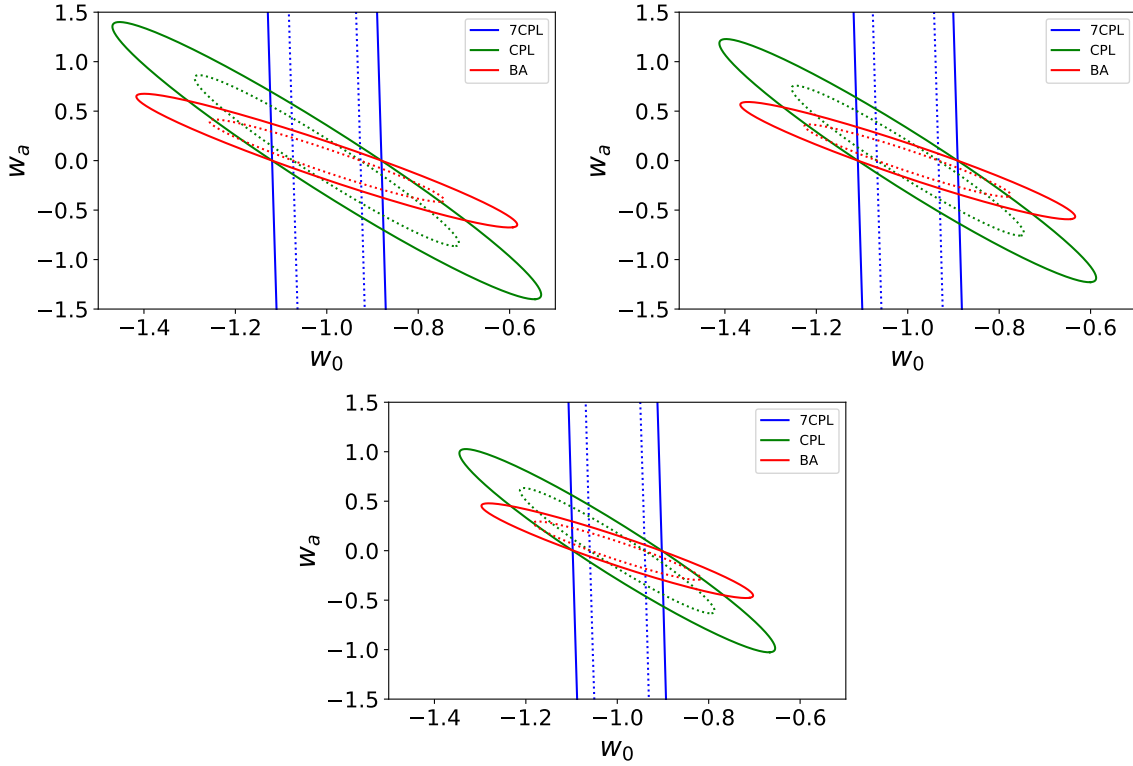


Figure 4: The 68% and 95% marginalized confidence intervals for the parameters w_0 and w_a from the Lyman- α convergence cross correlation for different dark energy EoS parametrizations. The fiducial model is chosen as the LCDM model with $(w_0, w_a) = (-1, 0)$. The three figures correspond to $\bar{n}_Q = 8 \text{ deg}^{-2}$, $\bar{n}_Q = 16 \text{ deg}^{-2}$ and $\bar{n}_Q = 100 \text{ deg}^{-2}$ respectively.

tion of state, 7CPL is definitely favourable than CPL or BA and the generally popular CPL parametrization may not be the best choice. It is also seen that the parameter space regions corresponding to $(w_0 > -1, w_a > 0)$ and $(w_0 < -1, w_a < 0)$ is constrained much better than the regions corresponding to $(w_0 > -1, w_a < 0)$ and $(w_0 < -1, w_a > 0)$. Thus regions which correspond to dark energy being modeled by only phantom or only non-phantom scalar fields are very strongly constrained.

6 Cross-correlation of CMBR weak-lensing with redshifted 21-cm signal

In a radio-interferometric observation the noise *rms.* in the real part in each visibility for single polarization measurement is given by

$$V_{rms} = \frac{T_{sys}}{K\sqrt{2\Delta\nu\Delta t}} \frac{\lambda^2}{2k_B} \quad (6.1)$$

Here k_B is the Boltzmann constant, $\Delta\nu$ is the width of the frequency channels and Δt is the integration time of the correlator. The total system temperature T_{sys} maybe decomposed as $T_{sys} = T_a + T_{sky}$, where T_a is an instrumental contribution and T_{sky} is a sky contribution which is usually subdominant and is given by [108]

$$T_{sky} = 60\text{K} \left(\frac{\nu}{300\text{MHz}} \right)^{-2.55}. \quad (6.2)$$

The quantity K denotes the antenna sensitivity and maybe written as $K = A_{eff}/2k_B$ where A_{eff} denotes the effective collecting area of each antenna. The factor $\frac{\lambda^2}{2k_B}$ intensity to temperature units in the Raleigh Jeans limit.

The noise variance in the visibility correlation is written as [101]

$$\sigma_{VV}^2 = \frac{8V_{rms}^4}{\mathcal{N}_p} \quad (6.3)$$

where \mathcal{N}_p is the number of visibility pairs in a particular visibility bin U to $U + \Delta U$. This is given by [69, 101]

$$\mathcal{N}_p = \frac{1}{2} \left[\frac{N_{ant}(N_{ant} - 1)}{2} \frac{T}{\Delta t} \Delta U^2 \rho(U, \nu) \right]^2 \frac{2\pi U \Delta U}{\Delta U^2} \quad (6.4)$$

where N_{ant} is the total number of antennas in the array, and T is the total observation time. The normalized baseline distribution function $\rho(U, \nu)$ is given by a convolution of the antenna distribution function with itself [109].

$$\rho(U, \nu) = \frac{c}{B} \int_0^\infty \rho_{ant}(\mathbf{r}) \rho_{ant}(\mathbf{r} - \lambda \mathbf{U}) \quad (6.5)$$

where B is the band width and c is fixed by the normalization $\int d^2\mathbf{U} \rho(\mathbf{U}) = 1$.

We consider Planck sensitivities for the cross-correlation. For the redshifted 21-cm observation we first consider a futuristic version of the upgraded GMRT (uGMRT) [110], with a larger number of antennas. The antenna distribution is roughly assumed to behave as $\rho_{ant}(r) \propto 1/r^2$ distributed over a $2 \times 2\text{Km}^2$ region. Each antenna is assumed to be of 45 m in diameter, with a field of view of 1.3° (FWHM). The frequency separation ν over which

Table 2: Specifications of the uGMRT like array used in the analysis

Observation time T (hrs)	Freq. range(MHz)	T_{sys} (K)	N_{ant}	ΔU	$A_{eff}(m^2)$
400	550-850	70	60, 100	32	1590

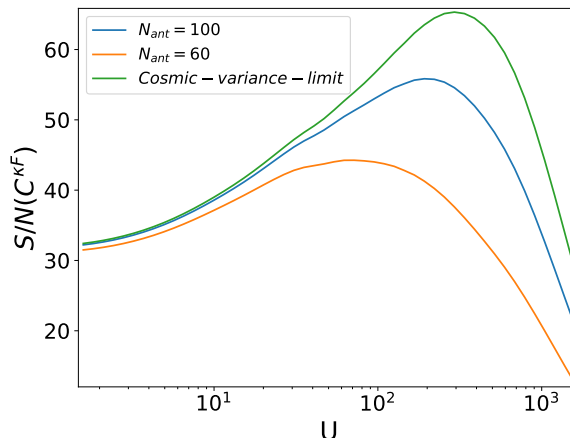


Figure 5: Signal to Noise ratio for the Convergence-21 cm cross angular power spectrum for the fiducial LCDM model for uGMRT like array with $N_{ant} = 60, 100$ respectively. We also show the cosmic variance limit.

the 21-cm signal remains correlated scales approximately as $\nu = 1\text{MHz}(\ell/100)^{-0.7}$ [101]. We assume that the signal is averaged over frequency bins of this width to increase the signal-to-noise ratio (S/N). The different telescope parameters used for our analysis is summarized in table (2).

Figure (5) shows the SNR for a LCDM fiducial model. We find that for a uGMRT like array with $N_{ant} = 60$ with LCDM fiducial model a peak SNR of ~ 40 is obtained at $\ell \sim 600$. If the number of antennas in the interferometer is $N_{ant} = 100$ a peak SNR of ~ 54 is achieved at $\ell \sim 1500$. In the limit of negligible instrumental noise a peak SNR of 70 is possible.

Figure (6) shows the difference of the 21-cm and CMBR convergence cross angular power spectrum for different dark energy EoS parametrizations from the cross angular power spectrum for the LCDM model. We find that BA, CPL and 7CPL models to be differentiable from the LCDM model at $> 3\sigma$ sensitivity.

For making more realistic error projections on $(w_0 - w_a)$, we also consider the radio interferometer MeerKAT [111]. This telescope has dishes of 13.5m diameter and a wider field of view. We consider the UHF-band of this telescope for our analysis. The telescope parameters for MeerKAT are summarized in the table (3).

Table 3: MeerKAT specifications

Observation time T (hrs)	Freq. range(MHz)	T_{sys} (K)	N_{ant}	ΔU	$A_{eff}/T_{sys}(m^2/K)$
400	580-1015	30	64	12	320

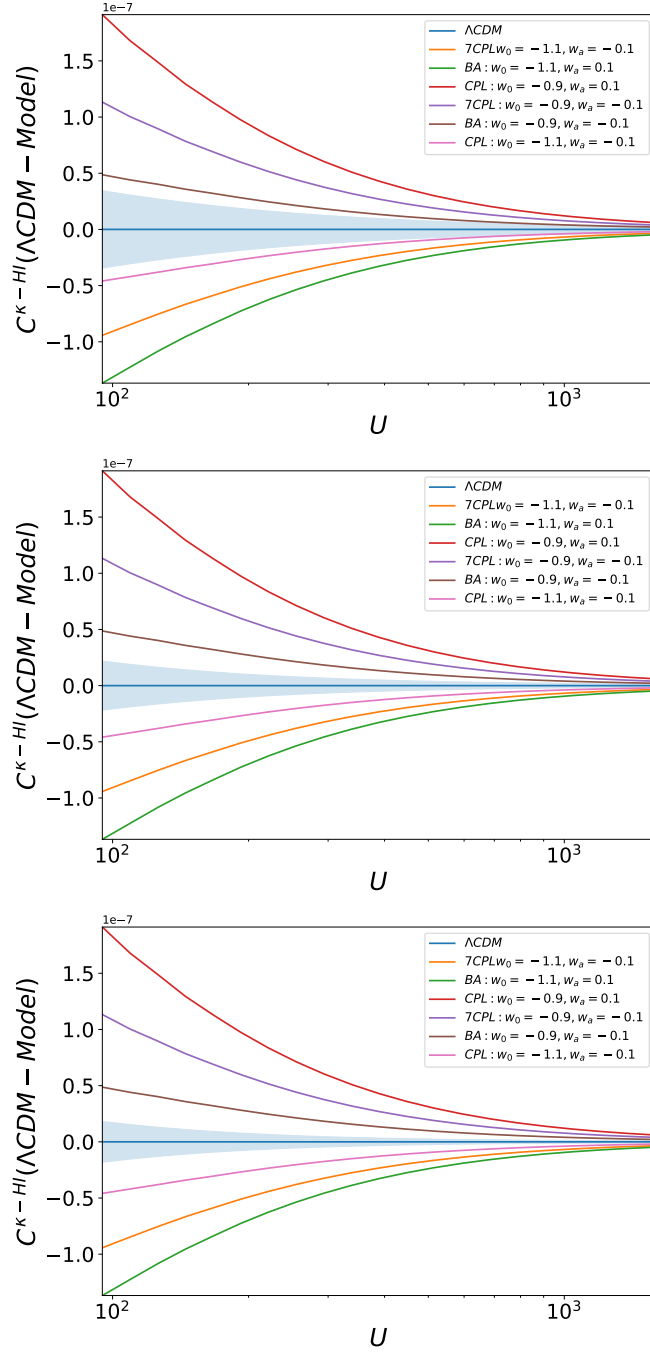


Figure 6: The difference of the 21 cm - convergence cross power spectrum for different fiducial dark energy parametrizations from the the ΛCDM model. The $1 - \sigma$ error is shown by the shaded region. The first and the second figure corresponds to a uGMRT like radio interferometer with $N_{ant} = 60$ and $N_{ant} = 100$ respectively. The observation time is 400 hrs. The last figure shows the best case scenario in the cosmic variance limit of no observational noise.

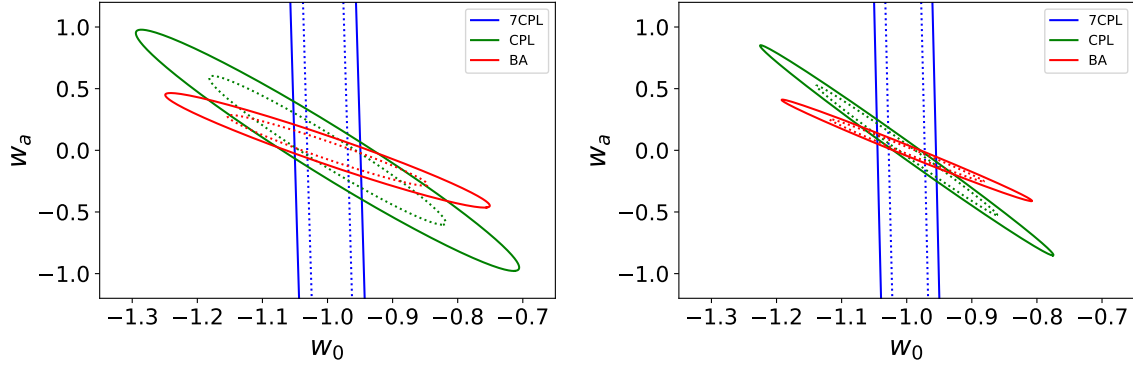


Figure 7: The 68% and 95% marginalized confidence intervals for the parameters w_0 and w_a from the 21-cm convergence cross correlation for different dark energy EoS parametrizations for uGMRT like telescope with $N_{ant} = 100$. The fiducial model is chosen as the LCDM model with $(w_0, w_a) = (-1, 0)$. The second figure shows the best case scenario of a cosmic variance dominated experiment.

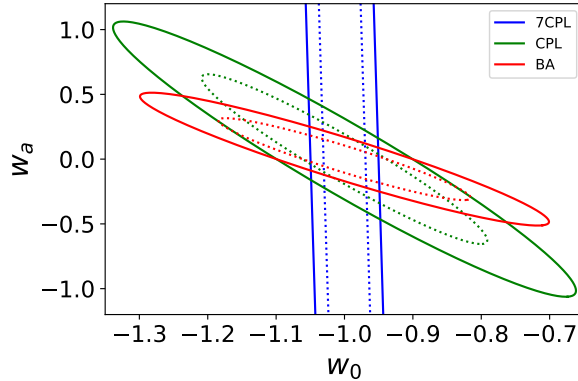


Figure 8: The 68% and 95% marginalized confidence intervals for the parameters w_0 and w_a from the 21-cm convergence cross correlation for different dark energy EoS parametrizations. The fiducial model is chosen as the LCDM model with $(w_0, w_a) = (-1, 0)$. The figures correspond to MeerKAT.

The Fisher matrix in Eq (4.30) is used to make error projections for the dark energy parameters. Fig (7) shows the constraints on the parameters in the $w_0 - w_a$ plane for cross-correlation with a uGMRT like telescope. The contours correspond to the 68% and 95% marginalized confidence intervals for the parameters w_0 and w_a . A summary of the errors obtained in the parameters (w_0, w_a) is given in the table(4). We find that the constraints on the EoS parameters are much better than the ones obtained from the cross-correlation with Lyman- α forest. This is due to the large bandwidth of the 21 cm observation over which the signal is averaged.

The results from cross-correlation with a more realistic MeerKAT is shown in the figure (8). The marginalized 1- σ errors obtained in the parameters (w_0, w_a) for MeerKAT is also given in the table(4). The constraints show reasonable degradation as compared to the

uGMRT predictions (with $N_{ant} = 100$).

Table 4: The 68% ($1 - \sigma$) Constraints of DE parameters (w_0, w_a) from HI 21-cm and convergence cross power spectrum

Model	Cosmic variance limit	uGMRT($N_{ant} = 100$)	MeerKAT
BA	$\Delta w_0 = 0.079, \Delta w_a = 0.121$	$\Delta w_0 = 0.098, \Delta w_a = 0.20$	$\Delta w_0 = 0.122, \Delta w_a = 0.22$
CPL	$\Delta w_0 = 0.092, \Delta w_a = 0.168$	$\Delta w_0 = 0.115, \Delta w_a = 0.40$	$\Delta w_0 = 0.138, \Delta w_a = 0.434$
7CPL	$\Delta w_0 = 0.04, \Delta w_a = --$	$\Delta w_0 = 0.05, \Delta w_a = --$	$\Delta w_0 = 0.053, \Delta w_a = --$

The projected constraints on the dark energy equation of state indicate that for a broad band 21-cm survey with uGMRT like telescope with 100 or more antennas the cross-correlation may constrain dark energy evolution at a level which is competitive with the projections for auto-correlation results with a SKA1 type experiment [54] or a joint Planck+SN+BAO+HST [107]. This is partly due to the fact that the projected instrumental noise levels with futuristic telescopes are not very high. However, we emphasize that in our analysis of cross-correlation of the tomographic field of 21-cm signal with the integrated weak lensing field, we have abandoned the line of sight information. By averaging the 21-cm signal along the radial direction, the SNR has improved considerably as compared to the usual tomographic 3-dimensional predictions from the auto-correlation.

The 7CPL parametrization is seen to constrain the present value of dark energy EoS much better than CPL and BA parametrization which is also the conclusion drawn in earlier works [54]. We also find that BA model constrains (w_0, w_a) much better than CPL model. Since CPL parametrization is the widely use parametrization to model dark energy evolution, we note that it may not be suitable to constrain dark energy evolution. The projection of (w_0, w_a) for CPL model has been studied extensively using eBOSS and DESI cosmological data [112, 113]. The limits of the error contours corresponding to the CPL model are $w_0 = (-1.5, -0.5)$, $w_a = (-1, 1)$ for the eBOSS survey which is similar to our projections. The PLANCK+DESI data limits for w_0 and w_a are $w_0 = (-1.13, -0.86)$ and $w_a = (-0.4, 0.4)$ respectively, which has better figure of merit. A comparison of dark energy EoS parameter error projections for different models are studied in the paper using Sne Ia JLA and BAO datasets [114]. Their projected error limits for the CPL model parameters are $\approx w_0 = (-1.6, -0.75)$ and $w_a = (-2.5, -1.5)$. Thus, we note that the cross-correlations between the weak lensing convergence with HI-21cm and Ly- α forest found better or reasonably close constraints on the w_0, w_a parameter space when compared with some other probes.

7 Conclusion

There are several observational aspects that we have not considered in this work. Foreground subtraction issues, is a major concern for the 21-cm signal. Large astrophysical foregrounds from galactic and extra galactic sources pose a serious threat towards achieving desired detection sensitivities [115]. Though the problem of foreground subtraction is less for the cross correlation, a significant amount of foreground subtraction is required to obtain good SNR since the foregrounds appear as noise in the cross-correlation. For the Lyman- α forest observations, continuum subtraction and avoiding metal line contamination, though less serious, needs to be carried out with high precision. Further, man made radio frequency interferences (RFIs), calibration errors and other systematics also needs to be tackled for a detection of

the HI 21-cm signal. We emphasize that some of the fundamental problems posed by 21-cm foregrounds can be avoided by considering cross correlations.

We also note that we have restricted our study of dark energy evolution to a very small set of commonly used parametrizations. There are a large number of possible 2-parameter descriptions which may suit some specific dark energy dynamics [83]. Though the CPL model and its variants fits a reasonable stretch of dark energy dynamics they do not describe all kinds of dynamics [116, 117]. We also note that the error projections obtained in this paper from a Fisher matrix analysis gives a good idea about the efficacy of the cross-correlation in constraining the (w_0, w_a) parameter space. However, a more sophisticated Bayesian analysis is needed for more robust statistical predictions.

We conclude by noting that the cross-correlation power spectrum of the HI tracers from the post reionization epoch with weak-lensing fields is a direct probe of cosmological structure formation which can be detected to a high level of statistical sensitivity with upcoming QSO surveys and radiointerferometers. This has the potential to provide new insights on dark energy evolution. This probe may be combined with other cosmological observations like CMB, BAO, SNIa etc and a joint analysis shall be able to give us a clearer picture of the nature of dark energy and its cosmic evolution.

References

- [1] L. Amendola and S. Tsujikawa, *Dark Energy: Theory and Observations*, Cambridge University Press (2010), [10.1017/CBO9780511750823](https://doi.org/10.1017/CBO9780511750823).
- [2] R. Durrer and R. Maartens, *Dark energy and modified gravity*, 2008.
- [3] S. Perlmutter, S. Gabi, G. Goldhaber, A. Goobar, D.E. Groom, I.M. Hook et al., *Measurements of the cosmological parameters omega and lambda from the first seven supernovae at $z > 0.35$* , *The Astrophysical Journal* **483** (1997) 565–581.
- [4] D.N. Spergel, L. Verde, H.V. Peiris, E. Komatsu, M.R. Nolte, C.L. Bennett et al., *First year wilkinson microwave anisotropy probe (wmap) observations: Determination of cosmological parameters*, *The Astrophysical Journal Supplement Series* **148** (2003) 175–194.
- [5] G. Hinshaw, D.N. Spergel, L. Verde, R.S. Hill, S.S. Meyer, C. Barnes et al., *First year wilkinson microwave anisotropy probe (wmap) observations: The angular power spectrum*, *The Astrophysical Journal Supplement Series* **148** (2003) 135–159.
- [6] M. Ata, F. Baumgarten, J. Bautista, F. Beutler, D. Bizyaev, M.R. Blanton et al., *The clustering of the SDSS-IV extended Baryon Oscillation Spectroscopic Survey DR14 quasar sample: first measurement of baryon acoustic oscillations between redshift 0.8 and 2.2*, *Monthly Notices of the Royal Astronomical Society* **473** (2017) 4773 [<https://academic.oup.com/mnras/article-pdf/473/4/4773/21941846/stx2630.pdf>].
- [7] T. Padmanabhan, *Cosmological constant—the weight of the vacuum*, *Physics Reports* **380** (2003) 235–320.
- [8] A.G. Riess, L.M. Macri, S.L. Hoffmann, D. Scolnic, S. Casertano, A.V. Filippenko et al., *A 2.4% determination of the local value of the hubble constant*, *The Astrophysical Journal* **826** (2016) 56.
- [9] G.-B. Zhao, M. Raveri, L. Pogosian, Y. Wang, R.G. Crittenden, W.J. Handley et al., *Dynamical dark energy in light of the latest observations*, *Nature Astronomy* **1** (2017) 627–632.
- [10] B. Ratra and P.J.E. Peebles, *Cosmological consequences of a rolling homogeneous scalar field*, *Phys. Rev. D* **37** (1988) 3406.

- [11] M.S. Turner and M. White, *Cdm models with a smooth component*, *Phys. Rev. D* **56** (1997) R4439.
- [12] R.R. Caldwell, R. Dave and P.J. Steinhardt, *Cosmological imprint of an energy component with general equation of state*, *Phys. Rev. Lett.* **80** (1998) 1582.
- [13] C. Armendariz-Picon, V. Mukhanov and P.J. Steinhardt, *Essentials of k-essence*, *Phys. Rev. D* **63** (2001) 103510.
- [14] M.C. Bento, O. Bertolami and A.A. Sen, *Generalized chaplygin gas, accelerated expansion, and dark-energy-matter unification*, *Phys. Rev. D* **66** (2002) 043507.
- [15] T. Padmanabhan and T.R. Choudhury, *Can the clustered dark matter and the smooth dark energy arise from the same scalar field?*, *Phys. Rev. D* **66** (2002) 081301.
- [16] S. Sen and A.A. Sen, *Late time acceleration in brans-dicke cosmology*, *Phys. Rev. D* **63** (2001) 124006.
- [17] J.S. Bagla, H.K. Jassal and T. Padmanabhan, *Cosmology with tachyon field as dark energy*, *Phys. Rev. D* **67** (2003) 063504.
- [18] F. Perrotta, C. Baccigalupi and S. Matarrese, *Extended quintessence*, *Phys. Rev. D* **61** (1999) 023507.
- [19] S. Nojiri, S.D. Odintsov and M. Sami, *Dark energy cosmology from higher-order, string-inspired gravity, and its reconstruction*, *Phys. Rev. D* **74** (2006) 046004.
- [20] J. Kujat, R.J. Scherrer and A.A. Sen, *Phantom dark energy models with negative kinetic term*, *Phys. Rev. D* **74** (2006) 083501.
- [21] R. Gannouji and M. Sami, *Galileon gravity and its relevance to late time cosmic acceleration*, *Phys. Rev. D* **82** (2010) 024011.
- [22] R.R. Caldwell and E.V. Linder, *Limits of quintessence*, *Physical Review Letters* **95** (2005) .
- [23] I. Maor, R. Brustein, J. McMahon and P.J. Steinhardt, *Measuring the equation of state of the universe: Pitfalls and prospects*, *Phys. Rev. D* **65** (2002) 123003.
- [24] S. Thakur, A. Nautiyal, A.A. Sen and T.R. Seshadri, *Thawing versus tracker behaviour: observational evidence*, *Monthly Notices of the Royal Astronomical Society* **427** (2012) 988 [<https://academic.oup.com/mnras/article-pdf/427/2/988/3006783/427-2-988.pdf>].
- [25] G. Pantazis, S. Nesseris and L. Perivolaropoulos, *Comparison of thawing and freezing dark energy parametrizations*, *Phys. Rev. D* **93** (2016) 103503.
- [26] M. CHEVALLIER and D. POLARSKI, *Accelerating universes with scaling dark matter*, *International Journal of Modern Physics D* **10** (2001) 213–223.
- [27] E.V. Linder, *Exploring the expansion history of the universe*, *Phys. Rev. Lett.* **90** (2003) 091301.
- [28] E. Barboza and J. Alcaniz, *A parametric model for dark energy*, *Physics Letters B* **666** (2008) 415–419.
- [29] M. Bartelmann and P. Schneider, *Weak gravitational lensing*, *Physics Reports* **340** (2001) 291–472.
- [30] L.V. Waerbeke and Y. Mellier, *Gravitational lensing by large scale structures: A review*, 2003.
- [31] D. MUNSHI, P. VALAGEAS, L. VANWAERBEKE and A. HEAVENS, *Cosmology with weak lensing surveys*, *Physics Reports* **462** (2008) 67–121.
- [32] L. Knox, A. Albrecht and Y.S. Song, *Weak lensing and supernovae: Complementary probes of dark energy*, 2004.

- [33] H. Hoekstra and B. Jain, *Weak gravitational lensing and its cosmological applications*, *Annual Review of Nuclear and Particle Science* **58** (2008) 99–123.
- [34] A. LEWIS and A. CHALLINOR, *Weak gravitational lensing of the cmb*, *Physics Reports* **429** (2006) 1–65.
- [35] W. Hu, *Mapping the dark matter through the cosmic microwave background damping tail*, *The Astrophysical Journal* **557** (2001) L79–L83.
- [36] U. Seljak and M. Zaldarriaga, *Measuring dark matter power spectrum from cosmic microwave background*, *Physical Review Letters* **82** (1999) 2636–2639.
- [37] W. Hu and T. Okamoto, *Mass reconstruction with cosmic microwave background polarization*, *The Astrophysical Journal* **574** (2002) 566–574.
- [38] M. Kamionkowski and E.D. Kovetz, *The quest for b modes from inflationary gravitational waves*, *Annual Review of Astronomy and Astrophysics* **54** (2016) 227–269.
- [39] J.S.B. Wyithe and A. Loeb, *The 21-cm power spectrum after reionization*, *MNRAS* **397** (2009) 1926.
- [40] S. Bharadwaj and S.K. Sethi, *HI Fluctuations at Large Redshifts: I–Visibility correlation*, *Journal of Astrophysics and Astronomy* **22** (2001) 293 [[arXiv:astro-ph/0203269](#)].
- [41] S. Bharadwaj, B.B. Nath and S.K. Sethi, *Using HI to Probe Large Scale Structures at $z = 3$* , *Journal of Astrophysics and Astronomy* **22** (2001) 21 [[arXiv:astro-ph/0003200](#)].
- [42] S. Wyithe and A. Loeb, *Fluctuations in 21cm Emission After Reionization*, *ArXiv e-prints* (2007) [[0708.3392](#)].
- [43] A. Loeb and J.S.B. Wyithe, *Possibility of Precise Measurement of the Cosmological Power Spectrum with a Dedicated Survey of 21cm Emission after Reionization*, *Physical Review Letters* **100** (2008) 161301 [[0801.1677](#)].
- [44] A.M. Wolfe, E. Gawiser and J.X. Prochaska, *Damped Ly-alpha Systems*, *ARAA* **43** (2005) 861 [[arXiv:astro-ph/0509481](#)].
- [45] J.X. Prochaska, S. Herbert-Fort and A.M. Wolfe, *The SDSS Damped Ly α Survey: Data Release 3*, *ApJ* **635** (2005) 123 [[arXiv:astro-ph/0508361](#)].
- [46] S.R. Furlanetto, S. Peng Oh and F.H. Briggs, *Cosmology at low frequencies: The 21cm transition and the high-redshift universe*, *Physics Reports* **433** (2006) 181–301.
- [47] J.R. Pritchard and A. Loeb, *21 cm cosmology in the 21st century*, *Reports on Progress in Physics* **75** (2012) 086901.
- [48] P. Bull, P.G. Ferreira, P. Patel and M.G. Santos, *Late-time cosmology with 21 cm intensity mapping experiments*, *The Astrophysical Journal* **803** (2015) 21.
- [49] S. Wyithe, A. Loeb and P. Geil, *Baryonic Acoustic Oscillations in 21cm Emission: A Probe of Dark Energy out to High Redshifts*, *ArXiv e-prints* (2007) [[0709.2955](#)].
- [50] T. Chang, U. Pen, J.B. Peterson and P. McDonald, *Baryon Acoustic Oscillation Intensity Mapping of Dark Energy*, *Physical Review Letters* **100** (2008) 091303 [[0709.3672](#)].
- [51] S. Bharadwaj, S.K. Sethi and T.D. Saini, *Estimation of cosmological parameters from neutral hydrogen observations of the post-reionization epoch*, *Physical Rev D* **79** (2009) 083538 [[0809.0363](#)].
- [52] Y. Mao, M. Tegmark, M. McQuinn, M. Zaldarriaga and O. Zahn, *How accurately can 21cm tomography constrain cosmology?*, *Physical Rev D* **78** (2008) 023529 [[0802.1710](#)].
- [53] A. Hussain, S. Thakur, T. Guha Sarkar and A.A. Sen, *Prospects of probing quintessence with hi 21cm intensity mapping survey*, *Monthly Notices of the Royal Astronomical Society* **463** (2016) 3492–3498.

- [54] B.R. Dinda, A.A. Sen and T.R. Choudhury, *Dark energy constraints from the 21cm intensity mapping surveys with SKA1*, *arXiv e-prints* (2018) arXiv:1804.11137 [[1804.11137](#)].
- [55] Y. Mao, M. Tegmark, M. McQuinn, M. Zaldarriaga and O. Zahn, *How accurately can 21 cm tomography constrain cosmology?*, *Physical Review D* **78** (2008) .
- [56] R.A.C. Croft, D.H. Weinberg, M. Pettini, L. Hernquist and N. Katz, *The power spectrum of mass fluctuations measured from the lyman alpha forest at $z = 2.5$* , *The Astrophysical Journal* **520** (1999) 1–23.
- [57] N.Y. Gnedin and A.J.S. Hamilton, *Matter power spectrum from the lyman-alpha forest: myth or reality?*, *Monthly Notices of the Royal Astronomical Society* **334** (2002) 107–116.
- [58] R. Mandelbaum, P. McDonald, U. Seljak and R. Cen, *Precision cosmology from the lyman alpha forest: power spectrum and bispectrum*, *Monthly Notices of the Royal Astronomical Society* **344** (2003) 776–788.
- [59] S. Gallerani, T.R. Choudhury and A. Ferrara, *Constraining the reionization history with qso absorption spectra*, *Monthly Notices of the Royal Astronomical Society* **370** (2006) 1401–1421.
- [60] P. McDonald and D.J. Eisenstein, *Dark energy and curvature from a future baryonic acoustic oscillation survey using the lyman alpha forest*, *Physical Review D* **76** (2007) .
- [61] J. Lesgourgues, M. Viel, M.G. Haehnelt and R. Massey, *A combined analysis of 3d weak lensing, lyman alpha forest and wmap year three data*, *Journal of Cosmology and Astroparticle Physics* **2007** (2007) 008–008.
- [62] A. Font-Ribera and SDSS-III Collaboration, *Cosmology from the BOSS Lyman-Alpha Forest*, in *American Astronomical Society Meeting Abstracts #225*, vol. 225 of *American Astronomical Society Meeting Abstracts*, p. 125.03, January, 2015.
- [63] T. Delubac, J.E. Bautista, N.G. Busca, J. Rich, D. Kirkby, S. Bailey et al., *Baryon acoustic oscillations in the lyman alpha forest of boss dr11 quasars*, *Astronomy and Astrophysics* **574** (2015) .
- [64] A. Font-Ribera, J. Miralda-Escudé, E. Arnau, B. Carithers, K.-G. Lee, P. Noterdaeme et al., *The large-scale cross-correlation of damped lyman alpha systems with the lyman alpha forest: first measurements from boss*, *Journal of Cosmology and Astroparticle Physics* **2012** (2012) .
- [65] M. McQuinn and M. White, *On estimating lyman alpha forest correlations between multiple sightlines*, *Monthly Notices of the Royal Astronomical Society* **415** (2011) 2257–2269.
- [66] T.G. Sarkar and K.K. Datta, *On using large scale correlation of the lyman alpha forest and redshifted 21-cm signal to probe hi distribution during the post reionization era*, *Journal of Cosmology and Astroparticle Physics* **2015** (2015) 001–001.
- [67] A. Garzilli, A. Magalich, T. Theuns, C.S. Frenk, C. Weniger, O. Ruchayskiy et al., *The lyman alpha forest as a diagnostic of the nature of the dark matter*, *Monthly Notices of the Royal Astronomical Society* **489** (2019) 3456–3471.
- [68] M. Viel, S. Matarrese, T. Theuns, D. Munshi and Y. Wang, *Dark energy effects on the lyman alpha forest*, *Monthly Notices of the Royal Astronomical Society* **340** (2003) L47–L51.
- [69] J.S. Bagla, N. Khandai and K.K. Datta, *Hi as a probe of the large-scale structure in the post-reionization universe*, *Monthly Notices of the Royal Astronomical Society* **407** (2010) 567–580.
- [70] T. Guha Sarkar, S. Mitra, S. Majumdar and T.R. Choudhury, *Constraining large-scale hi bias using redshifted 21-cm signal from the post-reionization epoch*, *Monthly Notices of the Royal Astronomical Society* **421** (2012) 3570–3578.
- [71] D. Sarkar, S. Bharadwaj and S. Anathpindika, *Modelling the post-reionization neutral hydrogen hi bias*, *Monthly Notices of the Royal Astronomical Society* **460** (2016) 4310–4319.

- [72] I.P. Carucci, F. Villaescusa-Navarro and M. Viel, *The cross-correlation between 21 cm intensity mapping maps and the Ly α forest in the post-reionization era*, *Journal of Cosmology and Astroparticle Physics* **2017** (2017) 001–001.
- [73] F. Villaescusa-Navarro, S. Genel, E. Castorina, A. Obuljen, D.N. Spergel, L. Hernquist et al., *Ingredients for 21 cm intensity mapping*, *The Astrophysical Journal* **866** (2018) 135.
- [74] T. Guha Sarkar, S. Bharadwaj, T.R. Choudhury and K.K. Datta, *Cross-correlation of the HI 21-cm signal and Lyman alpha forest: a probe of cosmology*, *Monthly Notices of the Royal Astronomical Society* **410** (2010) 1130–1134.
- [75] A.K. Sarkar, S. Bharadwaj and T.G. Sarkar, *Predictions for measuring the cross power spectrum of the HI 21-cm signal and the Lyman alpha forest using OWFA*, *Journal of Cosmology and Astroparticle Physics* **2018** (2018) 051–051.
- [76] A.K. Sarkar, A.K. Pal and T.G. Sarkar, *Constraining warm dark matter power spectrum using the cross-correlation of HI 21 cm signal and the Lyman- α forest*, *Journal of Cosmology and Astroparticle Physics* **2019** (2019) 058–058.
- [77] T.G. Sarkar, *CMB weak lensing and HI 21-cm cross-correlation angular power spectrum*, *Journal of Cosmology and Astroparticle Physics* **2010** (2010) 002–002.
- [78] A. Vallinotto, S. Das, D.N. Spergel and M. Viel, *Lenses in the forest: Cross correlation of the Lyman alpha flux with cosmic microwave background lensing*, *Physical Review Letters* **103** (2009) .
- [79] N. Aghanim, Y. Akrami, M. Ashdown, J. Aumont, C. Baccigalupi, M. Ballardini et al., *Planck 2018 results*, *Astronomy and Astrophysics* **641** (2020) 6.
- [80] E.V. Linder and D. Huterer, *How many dark energy parameters?*, *Phys. Rev. D* **72** (2005) 043509.
- [81] A. Albrecht, G. Bernstein, R. Cahn, W.L. Freedman, J. Hewitt, W. Hu et al., *Report of the Dark Energy Task Force, arXiv e-prints* (2006) astro [astro-ph/0609591].
- [82] R.J. Scherrer, *Mapping the Chevallier-Polarski-Linder parametrization onto physical dark energy models*, *Phys Rev D* **92** (2015) 043001 [1505.05781].
- [83] G. Pantazis, S. Nesseris and L. Perivolaropoulos, *Comparison of thawing and freezing dark energy parametrizations*, *Physical Review D* **93** (2016) 103503 [1603.02164].
- [84] K.M. Smith, A. Cooray, S. Das, O. Dore, D. Hanson, C. Hirata et al., *Gravitational lensing*, *AIP Conference Proceedings* (2009) .
- [85] K.M. Lanzetta, A.M. Wolfe and D.A. Turnshek, *The IUE Survey for Damped Lyman- α and Lyman-Limit Absorption Systems: Evolution of the Gaseous Content of the Universe*, *Astrophysical Journal* **440** (1995) 435.
- [86] C. Péroux, R.G. McMahon, L.J. Storrie-Lombardi and M.J. Irwin, *The evolution of Ω_{HI} and the epoch of formation of damped Lyman alpha absorbers*, *Monthly Notices of the Royal Astronomical Society* **346** (2003) 1103–1115.
- [87] P. Noterdaeme, P. Petitjean, C. Ledoux and R. Srianand, *Evolution of the cosmological mass density of neutral gas from Sloan Digital Sky Survey II – data release 7*, *Astronomy and Astrophysics* **505** (2009) 1087–1098.
- [88] T. Zafar, C. Péroux, A. Popping, B. Milliard, J.-M. Deharveng and S. Frank, *The ESO UES advanced data products quasar sample*, *Astronomy and Astrophysics* **556** (2013) A141.
- [89] L. Hui and N.Y. Gnedin, *Equation of state of the photoionized intergalactic medium*, *Monthly Notices of the Royal Astronomical Society* **292** (1997) 27–42.
- [90] H. Bi and A.F. Davidsen, *Evolution of structure in the intergalactic medium and the nature of the Lyman α forest*, *The Astrophysical Journal* **479** (1997) 523–542.

- [91] M. Viel, S. Matarrese, H. Mo, M. Haehnelt and T. Theuns, *Probing the intergalactic medium with the Lyman alpha forest along multiple lines of sight to distant quasars*, *Monthly Notices of the Royal Astronomical Society* **329** (2002) 848–862.
- [92] A. Slosar, S. Ho, M. White and T. Louis, *The acoustic peak in the Lyman alpha forest*, *Journal of Cosmology and Astroparticle Physics* **2009** (2009) 019–019.
- [93] A. Slosar, A. Font-Ribera, M.M. Pieri, J. Rich, J.-M.L. Goff, E. Aubourg et al., *The Lyman alpha forest in three dimensions: measurements of large scale flux correlations from BOSS 1st-year data*, *Journal of Cosmology and Astroparticle Physics* **2011** (2011) 001–001.
- [94] U. Seljak, *Bias, redshift space distortions and primordial non-gaussianity of nonlinear transformations: application to Ly-alpha forest*, *JCAP* **2012** (2012) 004 [[1201.0594](#)].
- [95] P. McDonald, *Toward a measurement of the cosmological geometry at $z \sim 2$: Predicting Ly alpha forest correlation in three dimensions and the potential of future data sets*, *The Astrophysical Journal* **585** (2003) 34–51.
- [96] A.M. Cieplak and A. Slosar, *Towards physics responsible for large-scale Lyman-alpha forest bias parameters*, *JCAP* **2016** (2016) 016 [[1509.07875](#)].
- [97] M.A. Fernandez, S. Bird and P. Upton Sanderbeck, *Effect of Separate Initial Conditions on the Lyman-alpha Forest in Simulations*, *arXiv e-prints* (2020) arXiv:2009.09119 [[2009.09119](#)].
- [98] S. Bird, K.K. Rogers, H.V. Peiris, L. Verde, A. Font-Ribera and A. Pontzen, *An emulator for the Lyman-alpha forest*, *JCAP* **2019** (2019) 050 [[1812.04654](#)].
- [99] S. Tanaka, S. Yoshiura, K. Kubota, K. Takahashi, A.J. Nishizawa and N. Sugiyama, *Detectability of CMB weak lensing and HI cross correlation and constraints on cosmological parameters*, 2020.
- [100] A.K. Sarkar, S. Bharadwaj and V.R. Marthi, *An analytical method to simulate the HI 21-cm visibility signal for intensity mapping experiments*, *Monthly Notices of the Royal Astronomical Society* **473** (2017) 261–270.
- [101] S. Bharadwaj and S.K. Pandey, *HI Fluctuations at Large Redshifts: II - the Signal Expected for the GMRT*, *Journal of Astrophysics and Astronomy* **24** (2003) 23 [[arXiv:astro-ph/0307303](#)].
- [102] D.P. Schneider, P.B. Hall, G.T. Richards, D.E.V. Berk, S.F. Anderson, X. Fan et al., *The Sloan Digital Sky Survey Quasar Catalog. III. Third Data Release*, *The Astronomical Journal* **130** (2005) 367.
- [103] K.S. Dawson and D.J.e. Schlegel, *The Baryon Oscillation Spectroscopic Survey of SDSS-III*, *Astrophysical Journal* **145** (2013) 10 [[1208.0022](#)].
- [104] F. Coppolani and P.e. Petitjean, *Transverse and longitudinal correlation functions in the intergalactic medium from 32 close pairs of high-redshift quasars**, *Monthly Notices of the Royal Astronomical Society* **370** (2006) 1804 [<https://academic.oup.com/mnras/article-pdf/370/4/1804/17316710/mnras0370-1804.pdf>].
- [105] V. D’Odorico, M. Viel, F. Saitta, S. Cristiani, S. Bianchi, B. Boyle et al., *Tomography of the intergalactic medium with Ly alpha forests in close quasar pairs*, *Monthly Notices of the Royal Astronomical Society* **372** (2006) 1333–1344.
- [106] G.D. Becker, P.C. Hewett, G. Worseck and J.X. Prochaska, *A refined measurement of the mean transmitted flux in the Lyman alpha forest using composite quasar spectra*, *Monthly Notices of the Royal Astronomical Society* **430** (2013) 2067 [<https://academic.oup.com/mnras/article-pdf/430/3/2067/13759836/stt031.pdf>].
- [107] Planck Collaboration, Ade, P. A. R., Aghanim, N., Arnaud, M. and A. et al., *Planck 2015 results - xiv. dark energy and modified gravity*, *Astronomy and Astrophysics* **594** (2016) A14.

- [108] A. Obuljen, E. Castorina, F. Villaescusa-Navarro and M. Viel, *High-redshift post-reionization cosmology with 21cm intensity mapping*, *Journal of Cosmology and Astroparticle Physics* **2018** (2018) 004–004.
- [109] K.K. Datta, S. Bharadwaj and T.R. Choudhury, *Detecting ionized bubbles in redshifted 21-cm maps*, *Monthly Notices of the Royal Astronomical Society* **382** (2007) 809 [<https://academic.oup.com/mnras/article-pdf/382/2/809/3432450/mnras0382-0809.pdf>].
- [110] Y. Gupta, B. Ajithkumar, H.S. Kale, S. Nayak, S. Sabhapathy, S. Sureshkumar et al., *The upgraded GMRT: opening new windows on the radio Universe*, *Current Science* **113** (2017) 707.
- [111] J. Jonas, *The meerkat radio telescope*, p. 001, 02, 2018, DOI.
- [112] G.-B. Zhao, Y. Wang, A.J. Ross, S. Shandera, W.J. Percival, K.S. Dawson et al., *The extended baryon oscillation spectroscopic survey: a cosmological forecast*, *Monthly Notices of the Royal Astronomical Society* **457** (2016) 2377–2390.
- [113] M. Vargas-Magana, D.D. Brooks, M.M. Levi and G.G. Tarle, *Unraveling the universe with desi*, 2019.
- [114] C. Escamilla-Rivera, *Status on bidimensional dark energy parameterizations using sne ia jla and bao datasets*, *Galaxies* **4** (2016) 8.
- [115] A. Ghosh, S. Bharadwaj, S.S. Ali and J.N. Chengalur, *Gmrt observation towards detecting the post-reionization 21-cm signal*, *Monthly Notices of the Royal Astronomical Society* **411** (2010) 2426–2438.
- [116] E.V. Linder, *The dynamics of quintessence, the quintessence of dynamics*, *General Relativity and Gravitation* **40** (2008) 329 [0704.2064].
- [117] Y. Wang and M. Tegmark, *New dark energy constraints from supernovae, microwave background, and galaxy clustering*, *Phys. Rev. Lett.* **92** (2004) 241302.
- [118] M. White, *Baryon oscillations*, *Astroparticle Physics* **24** (2005) 334–344.
- [119] D.J. Eisenstein, I. Zehavi, D.W. Hogg, R. Scoccimarro, M.R. Blanton, R.C. Nichol et al., *Detection of the baryon acoustic peak in the large-scale correlation function of sdss luminous red galaxies*, *The Astrophysical Journal* **633** (2005) 560–574.
- [120] W.J. Percival, S. Cole, D.J. Eisenstein, R.C. Nichol, J.A. Peacock, A.C. Pope et al., *Measuring the baryon acoustic oscillation scale using the sloan digital sky survey and 2df galaxy redshift survey*, *Monthly Notices of the Royal Astronomical Society* **381** (2007) 1053–1066.
- [121] L. Anderson, E. Aubourg and B. et.al, *The clustering of galaxies in the SDSS-III Baryon Oscillation Spectroscopic Survey: baryon acoustic oscillations in the Data Release 9 spectroscopic galaxy sample*, *Monthly Notices of the Royal Astronomical Society* **427** (2012) 3435 [<https://academic.oup.com/mnras/article-pdf/427/4/3435/2966997/427-4-3435.pdf>].
- [122] R.K. Sachs and A.M. Wolfe, *Perturbations of a Cosmological Model and Angular Variations of the Microwave Background*, *Astrophysical Journal* **147** (1967) 73.
- [123] S. Boughn and R. Crittenden, *A detection of the integrated sachs–wolfe effect*, *New Astronomy Reviews* **49** (2005) 75–78.
- [124] E. Komatsu, J. Dunkley, M.R.olta, C.L. Bennett, B. Gold, G. Hinshaw et al., *Five-year wilkinson microwave anisotropy probe observations: Cosmological interpretation*, *The Astrophysical Journal Supplement Series* **180** (2009) 330–376.
- [125] R. Scranton, A.J. Connolly, R.C. Nichol, A. Stebbins, I. Szapudi, D.J. Eisenstein et al., *Physical evidence for dark energy*, 2003.

- [126] N. Afshordi, Y.-S. Loh and M.A. Strauss, *Cross-correlation of the cosmic microwave background with the 2mass galaxy survey: Signatures of dark energy, hot gas, and point sources*, *Phys. Rev. D* **69** (2004) 083524.
- [127] T. Giannantonio, R. Scranton, R.G. Crittenden, R.C. Nichol, S.P. Boughn, A.D. Myers et al., *Combined analysis of the integrated sachs-wolfe effect and cosmological implications*, *Physical Review D* **77** (2008) .
- [128] T.G. Sarkar, K.K. Datta and S. Bharadwaj, *The cmb rsw and hi 21 cm cross-correlation angular power spectrum*, *Journal of Cosmology and Astroparticle Physics* **2009** (2009) 019–019.
- [129] W. Hu, *Lecture notes on cmb theory: From nucleosynthesis to recombination*, 2008.
- [130] K. Subramanian, *The physics of cmb anisotropies*, 2004.

Appendix

Background Evolution

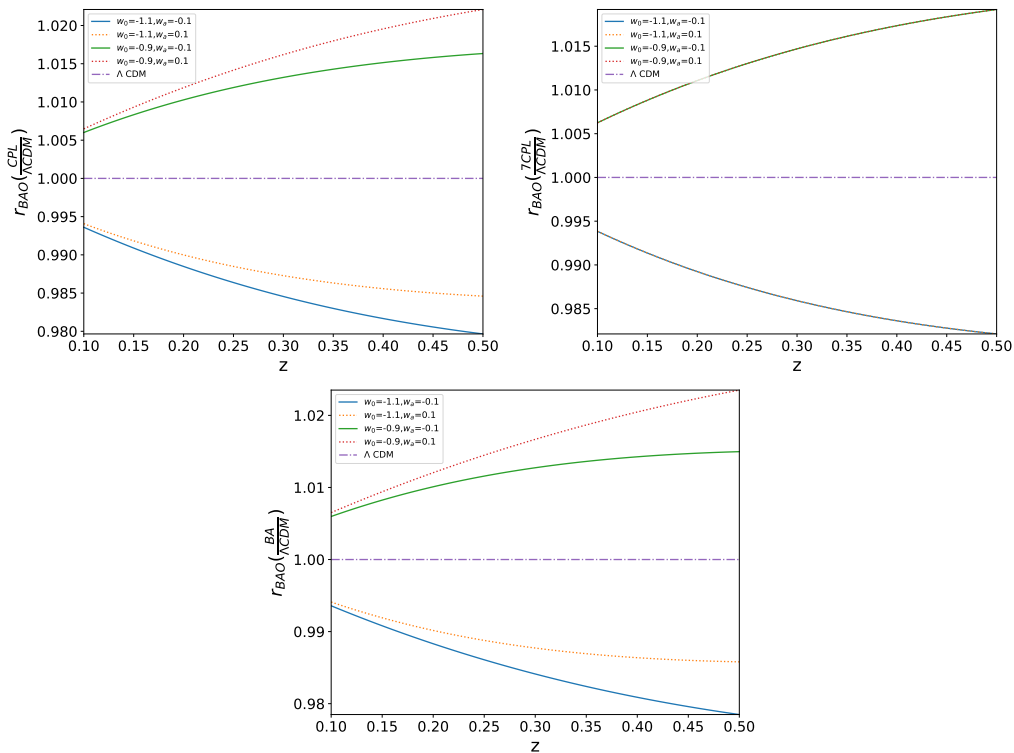


Figure 9: The BAO distance ratio $r_{BAO}(z)$ versus redshift z for different dark energy models (CPL, 7CPL, BA) in a spatially flat Universe scaled by $r_{BAO}(z)^{\Lambda CDM}$ for the ΛCDM model.

Baryon acoustic oscillation (BAO) observations [118] aim to constrain the angular diameter distance $d_A(z)$ and the Hubble parameter $H(z)$ through the imprint of the oscillatory feature of the matter power spectrum in the transverse (angular) and longitudinal directions respectively. Due to low SNR in BAO measurements, it is often convenient to measure an

effective distance defined as [1]

$$D_V(z) = \left[(1+z)^2 d_A(z)^2 \frac{cz}{H(z)} \right]^{1/3} \quad (7.1)$$

This effective distance is a direct quantifier of the background cosmological model (density parameters) and is thereby sensitive to the dynamical evolution of dark energy. We use a dimensionless quantifier of cosmological distances [119]

$$r_{BAO}(z) = \frac{r_s}{D_V(z)} \quad (7.2)$$

where r_s denotes the sound horizon at the recombination epoch. Figure (9) shows the departure of r_{BAO} as a function of z from the Λ CDM model prediction. A redshift dependent difference of a few percent from the Λ CDM model is seen for the different parametrizations. The behaviour is very similar for the CPL and BA parametrizations which are known to mimic the thawing class of dark energy models. The 7CPL parametrization which represents the tracking class shows identical behaviour for some sets of model parameters (see figure (9)). Observations from the 2df galaxy redshift survey gives the bounds on r_{BAO} as $r_{BAO}(z = 0.2) = 0.1980 \pm 0.0058$ and $r_{BAO}(z = 0.35) = 0.1094 \pm 0.0033$ [120]. All the models with a redshift dependent $w(z)$ seems to be in better agreement with this data. The analysis of BOSS (SDSS III) CMASS sample along with Luminous red galaxy sample [121] from SDSS-II gives $r_{BAO}(z = 0.57) = 0.07315 \pm 0.002$. Figure (10) shows the model predictions as compared to the data at different redshifts.

Growth of Perturbations

At sufficiently early times and on large spatial scales the matter density fluctuations are much less than unity ($|\delta| \ll 1$, in linear regime). Under these conditions the matter density contrast $\delta = \frac{\delta\rho_m}{\bar{\rho}_m}$ evolves independently for different Fourier modes k . Separating the time dependent part of the matter overdensity as $\delta(a) = D_+(a)\delta_m(a=1)$. The growth of density fluctuations on sub horizon scales can be obtained by solving the second order differential equation

$$\frac{d^2 D_+}{da^2} + \left(\frac{1}{H} \frac{dH}{da} + \frac{3}{a} \right) \frac{dD_+}{da} - \frac{3}{2} \frac{\Omega_{m_0} H_0^2}{a^5 H^2} D_+ = 0 \quad (7.3)$$

In order to solve the above equation we choose the initial conditions in the matter dominated epoch ($a_i = 10^{-3}$), where growth function grows linearly with the scale factor ($D_+ \propto a$).

Dark energy affects the growth of cosmological structure formation directly through the role of the expansion history on the gravitational instability in an expanding background. This leads to the appearance of the background evolution $H(z)$ in the equation for the growing mode of density perturbations D_+ (Eq: 7.3). We use the growth rate $f(z)$ defined as

$$f(z) = \frac{d \ln D_+}{d \ln a} \quad (7.4)$$

to quantify the growth rate of perturbations. The observationally measurable function $f(z)$ imprints the dynamics of dark energy and is sensitive to any departure from the Λ CDM model.

Figure (11), shows the linear growth rate of density perturbations for CPL, 7CPL and BA parametrizations. At higher redshifts, the all models approach $f \sim 1$ indicating that the

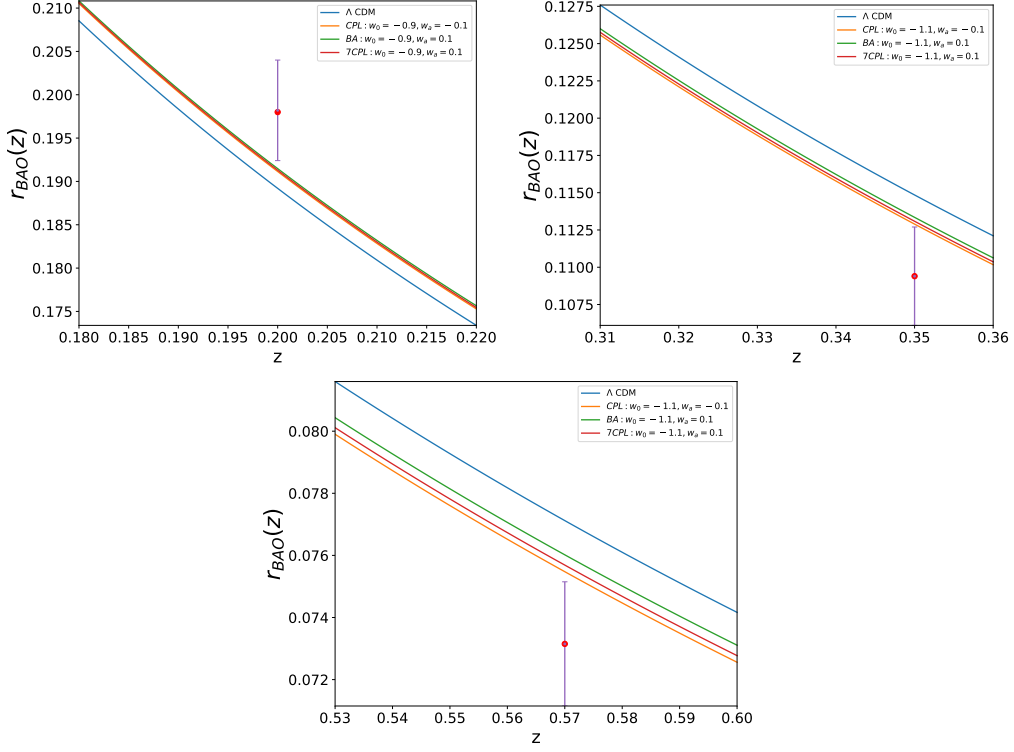


Figure 10: The first two figures in the panel shows the data points from the 2df galaxy survey at redshifts $z = 0.2$ and $z = 0.35$ respectively and the third figure shows the high redshift data at $z = 0.57$ from BOSS SDSS-III survey.

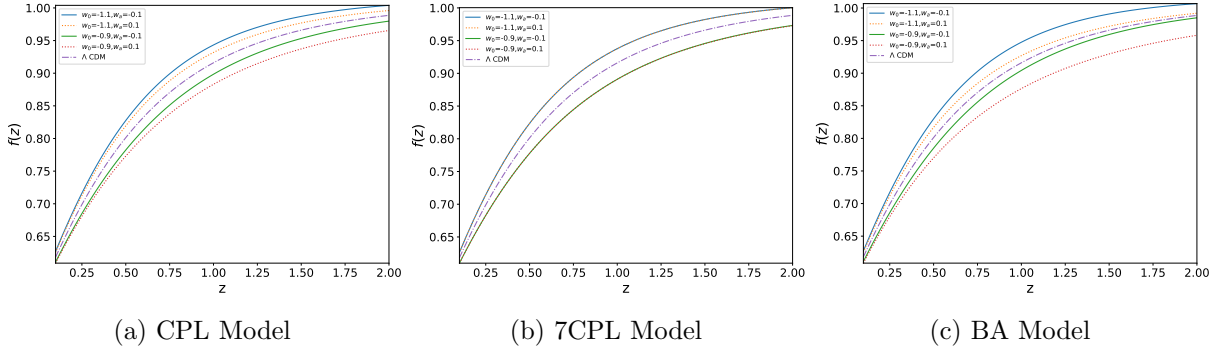


Figure 11: The growth rate of density fluctuations $f(z)$ for different dark energy EoS parametrizations. The Λ CDM model is shown in each subfigure for comparison.

growth of perturbation is dominated by non-relativistic matter. Further, for 7CPL model, there is no dependence of the parameter w_a . Therefore, one does not expect to constrain the parameter w_a for 7CPL model using any observation related to matter clustering.

Dark energy also has an implicit observational effect. It causes a decay of the gravitational potential (the scalar perturbation in the Newtonian conformal gauge), when the

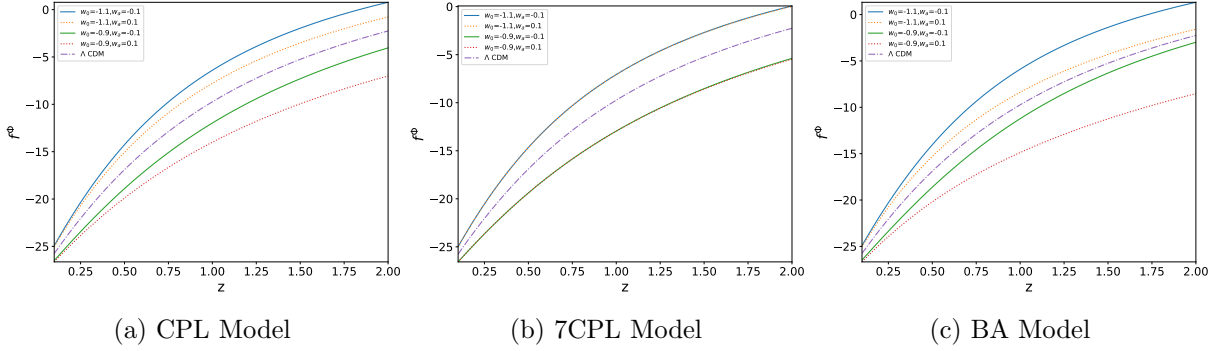


Figure 12: The ISW parameter $f^\Phi = \frac{\dot{\Phi}}{\Phi}$ for different dark energy EoS parametrizations. The Λ CDM model is shown in each subfigure for comparison.

Universe evolves from the matter dominated to the dark energy dominated era. This is known to generate a weak anisotropy in the CMB temperature fluctuation, through the Integrated Sachs Wolfe (henceforth ISW) effect [122, 123]. A curved spatial geometry also similarly contributes to this anisotropy. However, the spatial curvature of our Universe is constrained to be zero from CMBR observations [124] whereby the effect of spatial curvature can be ignored in the first approximation. The gravitational potential is expected to remain constant in a purely matter dominated cosmology. Thus, any late-time evolution of the gravitational potential is sensitive to the dark energy model [125–128]. The ISW anisotropy is a line of sight integral [129, 130]

$$\Delta T(\hat{\mathbf{n}})^{\text{ISW}} = 2T \int_{\eta_{\text{LSS}}}^{\eta_0} d\eta \Phi'(r\hat{\mathbf{n}}, \eta) \quad (7.5)$$

where T is the present CMBR temperature, η_{LSS} and η_0 are the conformal times at the last scattering surface and the present epoch respectively and $\Phi' = d\Phi/d\eta$. To quantify this effect we define a diagnostic for dark energy

$$f^\Phi(z) = \frac{d}{d\eta} \ln \Phi = (f - 1)\mathcal{H} \quad (7.6)$$

where $\mathcal{H} = \frac{1}{a} da/d\eta$. It is known that $f \sim 1$ in pure matter dominated epoch and any departure from $f = 1$ indicates the action of dark energy. Noting that the role of dark energy is imprinted in $f - 1$, the function $f^\Phi(z)$ is a sensitive probe of dark energy. It quantifies the interplay of two time scales - the background expansion rate (contained in $H(z)$) and the growth rate of cosmological structure (contained in $f(z)$).

Figure(12) shows the redshift dependence of $f^\Phi(z)$ for different dark energy EoS parametrizations. The 7CPL model shows insensitivity to the parameter w_a , however both CPL and BA parametrizations show significant $\sim 2 - 4\%$ departure from the Λ CDM behaviour. This may be crucial in the improvement of detection sensitivities for ISW measurements [128].